Microbiology and Infectious Disease

On the Role of VP3-PI3P Interaction in Birnavirus Endosomal Membrane Targeting

Reviewed Preprint
v2 • February 5, 2025
Revised by authors

Reviewed Preprint
v1 • April 26, 2024

Flavia A Zanetti, Ignacio Fernández, Eduard Baquero, Pablo Guardado-Calvo, Andres Ferrino-Iriarte, Sarah Dubois, Etienne Morel, Victoria Alfonso, Milton O Aguilera, María E Celayes, Luis M Polo, Laila Suhaiman, Vanesa V Galassi, María V Chiarpotti, Carolina Allende, Javier M Rodríguez, José R Castón, Diego Lijavetzky, Oscar Taboga, María I Colombo, Mario G Del Pópolo, Félix A Rey, Laura R Delgui

Instituto de Ciencia y Tecnología "Dr. Cesar Milstein", Consejo Nacional de Investigaciones Científicas y Técnicas (CONICET), Buenos Aires, Argentina • Institut Pasteur, Université Paris Cité, Structural Virology Unit, Paris, France • Université Paris Cité, INSERM UMR-S1151, CNRS UMR-S8253, Institut Necker Enfants Malades, Paris, France • Instituto de Agrobiotecnología y Biología Molecular (IABIMO), Instituto Nacional de Tecnología Agropecuaria (INTA), Consejo Nacional de Investigaciones Científicas y Técnicas (CONICET), Buenos Aires, Argentina • Instituto de Histología y Embriología de Mendoza, Universidad Nacional de Cuyo (UNCuyo), Consejo Nacional de Investigaciones Científicas y Técnicas (CONICET), Centro Universitario M5502JMA, Mendoza, Argentina • Instituto Interdisciplinario de Ciencias Básicas (ICB), Consejo Nacional de Investigaciones Científicas y Técnicas (CONICET), Mendoza, Argentina • Facultad de Ciencias Exactas y Naturales, Universidad Nacional de Cuyo (UNCuyo), Mendoza, Argentina • Department of Structure of Macromolecules, Centro Nacional de Biotecnología (CNB-CSIC), Madrid, Spain • Instituto de Biología Agrícola de Mendoza, Universidad Nacional de Cuyo (UNCuyo), Consejo Nacional de Investigaciones Científicas y Técnicas (CONICET), Mendoza, Argentina

https://en.wikipedia.org/wiki/Open_access
Copyright information

eLife Assessment

Zanetti et al use **convincing** biophysical and cellular assays to investigate the interaction of the birnavirus VP3 protein with the early endosome lipid PI3P. The study provides **valuable** insights and will be of interest to virologists. In future studies, it would be interesting to demonstrate that VP3-PIP3P is a specific interaction and not a general interaction with other PIPs.

https://doi.org/10.7554/eLife.97261.2.sa3

Abstract

Birnaviruses are a group of double-stranded RNA (dsRNA) viruses infecting birds, fish and insects. Early endosomes (EE) constitute the platform for viral replication. Here, we study the mechanism of birnaviral targeting of EE membranes. Using the Infectious Bursal Disease Virus (IBDV) as a model, we validate that the viral protein 3 (VP3) binds to phosphatidylinositol-3-phosphate (PI3P) present in EE membranes. We identify the domain of VP3 involved in PI3P-binding, named P2 and localized in the core of VP3, and establish the critical role of the arginine at position 200 (R_{200}), conserved among all known birnaviruses. Mutating R_{200} abolishes viral replication. Moreover, we propose a two-stage modular

mechanism for VP3 association with EE. Firstly, the carboxy-terminal region of VP3 adsorbs on the membrane, and then the VP3 core reinforces the membrane engagement by specifically binding PI3P through its P2 domain, additionally promoting PI3P accumulation.

Significance Statement

Birnaviruses are a family of viruses unique among the group of dsRNA viruses. Here, we show that VP3 seizes the endosomes by anchoring to the PI3P lipids in the luminal side of the EE membrane, in order to organize the viral replication factory. We propose a two-stage modular mechanism for VP3 association with PI3P-enriched EE. The significance of this work resides in the biochemical and biophysical insights on the mechanism of association of VP3 with EE and its role in the viral life cycle, which represents a substantial contribution toward understanding the replication strategy of these "*non-canonical*" viruses.

Introduction

Birnaviruses belong to the *Birnaviridae* family composed of nonenveloped icosahedral dsRNA viruses that infect a wide range of vertebrate and invertebrate hosts. The prototypical and best-characterized family member, the Infectious Bursal Disease Virus (IBDV), is the causative agent of Gumboro disease, a highly contagious immunosuppressive disease that affects young chickens (*Gallus gallus*) causing significant damage to the poultry industry (Delmas et al., 2019).

Birnaviruses are unconventional dsRNA viruses, as the virions lack a "*core*", i.e., an inner protein layer containing the genome, which instead forms a filamentous ribonucleoprotein complex (RNP) with the multifunctional protein VP3, the RdRp VP1, and the dsRNA genome segments (Luque et al., 2009b). IBDV contains a single ~70-nm diameter T = 13*l* icosahedral capsid surrounding a polyploid bipartite dsRNA genome (segments A and B, 3.2 and 2.8 kbp, respectively) (Luque et al., 2009a). The X-ray crystal structure of the capsid revealed that VP2 is the only component. VP2 has two main domains, a "shell" domain homologous to the coat proteins of +sRNA such as the T = 3 nodaviruses, and a "tower" domain, like those present in the T = 13 middle-layer protein of dsRNA viruses of the order *Reovirales* (Coulibaly et al., 2005). VP3 is a 257-residues long polypeptide that plays multiple roles during the viral life cycle. In the mature virion, VP3 is a component of the RNPs, where it is associated with the dsRNA (Luque et al., 2009b). During viral assembly, VP3 acts as a scaffold protein via electrostatic interactions between basic residues of pVP2 (the precursor form of VP2), and acidic residues at the VP3 carboxy-terminal (Ct) region (Saugar et al., 2010). Additionally, VP3 interacts with VP1 (Lombardo et al., 1999). VP3's multifunctional properties might be mediated by its capacity to form oligomers (Casañas et al., 2008), or by its intrinsically disordered regions. The X-ray crystal structure of the central region of the IBDV VP3 (residues 82 to 222) showed that it consists entirely of α-helices connected by loops which can be divided into two structural domains linked by a flexible hinge. The 36 Ct residues of the protein, a highly hydrophilic region rich in charged amino acids and proline residues, were predicted to be disordered, so it was excluded from the crystallized construct. The 81 amino-terminal (Nt) region of VP3 was cleaved during the crystallization process and was absent in the crystal (Casañas et al., 2008). The X-ray crystal structure indicated the presence of two positively charged domains, termed Patch 1 (P1) and Patch 2 (P2) (Valli et al., 2012). Both patches are composed of four discontinuous, positively charged residues forming two exposed patches on the surface of the protein. P1 was demonstrated to be involved in the dsRNA binding-activity of VP3 (Valli et al., 2012).

Previous studies on the subcellular localization of the IBDV replication complex (RC) have shown that IBDV replication components are localized to EE (Delgui et al., 2013). Further analysis revealed that VP3 associates with the cytosolic leaflet of EE membranes via P2, with a critical functional role in the virus life cycle (Gimenez et al., 2018). Additionally, the presence of PI3P in EE membranes was demonstrated to be a key host factor for VP3 association and the consequent establishment of IBDV RCs on EE membranes (Gimenez et al., 2020).

Here we study the mechanism mediating the birnaviral targeting of EE membranes, focusing on the VP3-PI3P interaction. Using biophysical approaches in cell-free *in vitro* systems, we demonstrate that PI3P constitutes the cellular partner for VP3 association to EE membranes. By introducing charge-reversal point mutations on VP3 P2, we establish the contribution of each of the four positively charged residues composing P2, with a key role of the arginine at position 200 (R_{200}), a residue conserved across all known birnaviruses. Using a reverse genetic system for IBDV, we show that mutating R_{200} abolishes viral replication. Finally, by using molecular simulations, we discuss a potential two-stage modular mechanism for VP3 association with EE. We show that, in the first step, the Ct flexible tail of VP3 adsorbs to the membrane by electrostatic interactions due to its positive charge. Then, in the second stage, the VP3 core reinforces the membrane engagement by recruiting PI3P molecules scattered in the EE membrane to the P2 region, promoting a stable VP3-PI3P interaction.

Results

Biophysical characterization of VP3 binding to PI3P

We set up a liposome co-flotation assay to assess the binding of VP3 to PI3P in membranes. We expressed and purified His-tagged VP3 full-length (His-VP3 FL) and confirmed its identity by Western blot using specific anti-VP3 and anti-His antibodies. Since we observed four different bands for the purified protein, we confirmed their VP3-identity by mass spectrometry (*SI Appendix*, Fig. S1). We prepared two populations of liposomes: "liposomes PI3P(-)" and "liposomes PI3P(+)". We confirmed that these preparations were suitable for evaluating the interaction with PI3P by monitoring co-flotation of a recombinant His-2xFYVE domain (Fab1p, YOTB, Vac1p, and EEA1), followed by immunoblot detection of the His-tag. FYVE domains are highly homologous cysteine-rich domains of 70-80 amino acids present in around 30 human proteins that are known to participate in vesicular sorting or endocytosis through direct binding to PI3P from EE (Burd and Emr, 1998; Gaullier et al., 1998; Simonsen et al., 1998; Stenmark et al., 1996) (**Fig. 1A**). We observed specific binding of His-VP3 FL to liposomes PI3P(+), evidenced by a significant difference in the ability to bind to both liposome populations (**Fig. 1B**). To test His-VP3 FL PI3P-binding specificity, we performed a co-flotation assay using liposomes where PI3P was replaced by 1,2-dioleoyl-sn-glycero-3-phosphate ("liposomes PA") or [1,2-dioleoyl-sn-glycero-3-phospho-(1'-myo-inositol)] ("liposomes PI") at the same molar ratio. PA contains a POH^- group also present in the polar head of PI3P but lacks the inositol ring, while PI has the inositol ring but is not phosphorylated. We observed that His-VP3 FL bound to liposomes PI3P(+), but not to liposomes PA or PI, reinforcing the notion that a phosphoinositide is required since neither a single negative charge nor an inositol ring are sufficient to promote VP3 binding to liposomes (*SI Appendix*, Fig. S2).

Two additional biophysical approaches were implemented. First, we prepared liposomes PI3P(-) and PI3P(+), and incubated them with His-2xFYVE or His-VP3 FL that had been pre-bound to Ni-NTA [nickel (II) nitrilotriacetic acid] gold particles. Subsequently we inspected the preparations by cryo-electron microscopy (cryo-EM). Gold particles were not observed on liposomes PI3P(-) incubated with either protein (**Fig, 1C, left panel**). We observed gold particles decorating liposomes PI3P(+) in the presence of both, His-2xFYVE and His-VP3 FL (**Fig. 1C, right panel**). Second, we performed bio-layer interferometry (BLI) experiments using purified His-VP3 FL, and

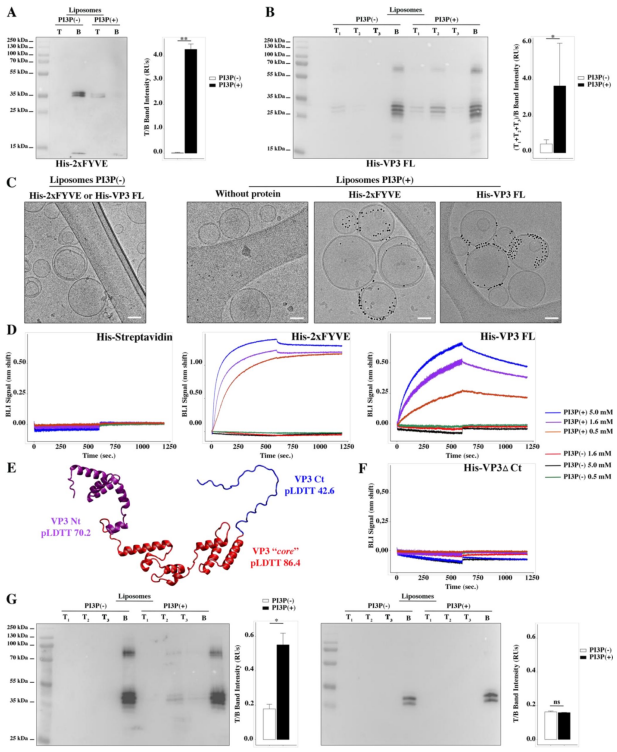

Figure 1.

Biophysical characterization of VP3 binding to PI3P.

(A) Immunoblots of the top (T) and bottom (B) fractions from a liposome PI3P(-) or PI3P(+) OptiprepTM co-floatation assay indicating that His-2xFYVE protein (~35 kDa) specifically binds to liposome PI3P(+). Results are representative of three independent experiments. The bar plot represents the intensity of T/B bands for each liposome preparation. Significant differences (** P <0.01) as determined by one-way ANOVA with Tukey's HSD test.
(B) Immunoblots of the three top (T_1, T_2 and T_3) and bottom (B) fractions from a liposome PI3P(-) or PI3P(+) OptiprepTM co-floatation assay indicating that His-VP3 FL protein (~32 kDa) specifically binds to liposome PI3P(+). Results are representative of three independent experiments. The bar plot represents the intensity of (T_1+T_2+T_3)/B bands for each liposome preparation. Significant differences (* P <0.05) as determined by one-way ANOVA with Tukey's HSD test.
(C) Liposomes were vitrified and only representative cryo-electron microscopy images are shown. Left panel: liposomes PI3P(-) incubated even with the Ni-NTA gold particles reagent alone or pre-incubated with His-2xFYVE of His-VP3 FL. Right panel: liposomes PI3P(+) control (without protein), or incubated with His-2xFYVE-or His-VP3 FL-Ni-NTA gold particles showing gold particles decorating the membrane of the liposomes when His-2xFYVE or His-VP3 FL were present. The bar represents 50 nm.
(D) Binding of His-Streptavidin (negative control), His-2xFYVE (positive control) or His-VP3 FL to three different concentrations of liposomes PI3P(-) or PI3P(+). Association and dissociation sensorgrams measured by bio-layer interferometry (BLI), showing the specific interaction of His-2xFYVE and His-VP3 FL with liposomes PI3P(+) in a dose-dependent manner, as indicated.
(E) Cartoon representation of AlphaFold2 prediction of VP3 FL. Red region corresponds to the "*core*" region of the protein present in the experimental X-ray crystallographic model obtained by Casañas and coworkers [PDB: 2R18 (Casañas et al., 2008)]. Regions not present within the PDB are colored in violet and blue representing the Nt and the Ct of VP3, respectively. pLDTT values lower than 50 are a strong predictor of disorder.
(F) Binding of His-VP3 DCt to three different concentrations of liposomes PI3P(-) or PI3P(+). Sensorgrams measured by BLI, showing the absence of binding to either liposomes when the VP3 lacks the Ct region [blue in (E)].
(G) Immunoblots of the three top (T_1, T_2 and T_3) and bottom (B) fractions from a liposome PI3P(-) or PI3P(+) OptiprepTM co-floatation assay of His-VP3 FL protein (~32 kDa) (positive control, left panel) or His-VP3 DCt protein (~28 kDa) (right panel) showing the lack of VP3 DCt binding to both liposomes. Results are representative of three independent experiments. The bar plot represents the intensity of (T_1+T_2+T_3)/B bands for each liposome preparation. Significant differences (* P <0.05; ns P >0.05) as determined by one-way ANOVA with Tukey's HSD test.

liposomes PI3P(-) and PI3P(+) (Shah et al., 2014). In the BLI experiments, the protein is immobilized on the tip of Ni-NTA sensors while the liposomes remain in solution, allowing to monitor the molecular interactions in real-time (Kairys et al., 2019). Purified His-Streptavidin and His-2xFYVE were used as negative and positive controls, respectively. A specific liposome PI3P(+) dose-dependent binding of His-2xFYVE and His-VP3 FL was observed (**Fig. 1D**).

Previous studies indicated that the P2 is responsible for PI3P binding on EE membranes (Gimenez et al., 2020, 2018). Yet the Ct region of VP3 is also highly enriched in positively charged residues. We generated a computational model of FL VP3 using AlphaFold2 (Jumper et al., 2021), which predicted a disordered Ct region (pLDTT of 42.6) (**Fig. 1E**). Thus, we hypothesized that both conditions, the positive electrostatic surface charge and the disordered character of the VP3 Ct, might be contributing to the binding to the surface of EE. To test this hypothesis, we made a VP3 construct bearing a Ct truncation (His-VP3 ΔCt) and used it in co-flotation assays and BLI experiments. We did not detect interaction of this mutant with PI3P(-) nor PI3P(+) liposomes (**Fig. 1F, G**). Taken together, our results validate the role of PI3P in the interaction with VP3 and underscore the significance of the Ct domain in mediating this interaction.

Role of VP3 P2 in the association of VP3 with the EE membrane

Inspection of the VP3 crystal structure showed that P2 residues (K_{157}, R_{159}, H_{198} and R_{200}) form a positive-charged groove on the protein surface (**Fig. 2A-B**). We prepared VP3 point mutants with reversed charge in a pcDNA vector backbone, giving rise to pcDNA VP3 K_{157}D, R_{159}D, H_{198}D and R_{200}D. The calculated electrostatic potential of P2 for each of these mutants is shown in **Fig. 2C**. Firstly, we used QM7 cells transiently overexpressing VP3 P2 Wild Type (WT), P2 (all reversed) or the four single mutation of P2 to quantitatively assess their cellular distribution. We observed a punctuated distribution of VP3 P2 WT, K_{157}D, R_{159}D and H_{198}D. In contrast, the specific indirect immunofluorescence (IIF) signal of VP3 P2 all reversed and R_{200}D showed a diffuse cytosolic distribution (**Fig. 2D, panels framed in red**). Secondly, we assessed the distribution of the VP3 constructs in QM7 cells transiently overexpressing EGFP-Rab5. Rab5 regulates the homotypic tethering and fusion of EEs, and it is considered a genuine marker of EEs (Gorvel et al., 1991). As observed in **Fig. 2E**, and the quantitative colocalization analysis (*SI Appendix*, Fig. S3), VP3 P2 WT, K_{157}D, R_{159}D and H_{198}D showed a marked colocalization with EGFP-Rab5. In contrast, the VP3 P2 all reversed and R_{200}D-derived IIF signal indicated a cytosolic distribution (**Fig. 2E, panels framed in red**). It is important to mention that the differences in co-localization shown in Fig. S3 are small and not significant, but still show a trend that correlates with observations depicted in **Fig. 2D**. Taken together, these results suggest that R_{200} in the P2 patch bears a critical role in the association of VP3 with EE membranes.

VP3 P2 mediates VP3-PI3P association to EE membranes

To further assess the contribution of P2 residues to PI3P binding, and to strengthen the observations made on cells transiently overexpressing EGFP-Rab5, we set up two additional cell biology assays. One consists of co-transfecting cells with EGFP-2xFYVE and VP3 constructs, and detecting them by confocal laser scanning microscopy (CLSM). The second one consists of assessing the ability of purified GST-2xFYVE, which recognizes endogenous PI3P, to co-localize with VP3. We employed QM7 cells transiently co-overexpressing EGFP-2xFYVE and VP3 P2 WT, P2 all reversed, or the four point mutants to evaluate their colocalization. As shown in **Fig. 3A**, we observed a punctuated distribution with a marked co-localization with EGFP-2xFYVE for VP3 P2 WT while for VP3 P2 all reversed the IIF signal indicated a cytosolic distribution of the protein with the loss of colocalization with EGFP-2xFYVE (**Fig. 3A, red framed panels on the upper two rows**). Regarding the point mutants, we observed a loss of punctuated distribution and EGFP-2xFYVE co-localization for VP3 FL R_{200}D (**Fig. 3A, red framed panels on the bottom row**). Then, we used the GST-2xFYVE purified domain to recognize endogenous PI3P in fixed cells (Nascimbeni et al., 2017). GST-2xFYVE was used as the “primary antibody”, which was labelled

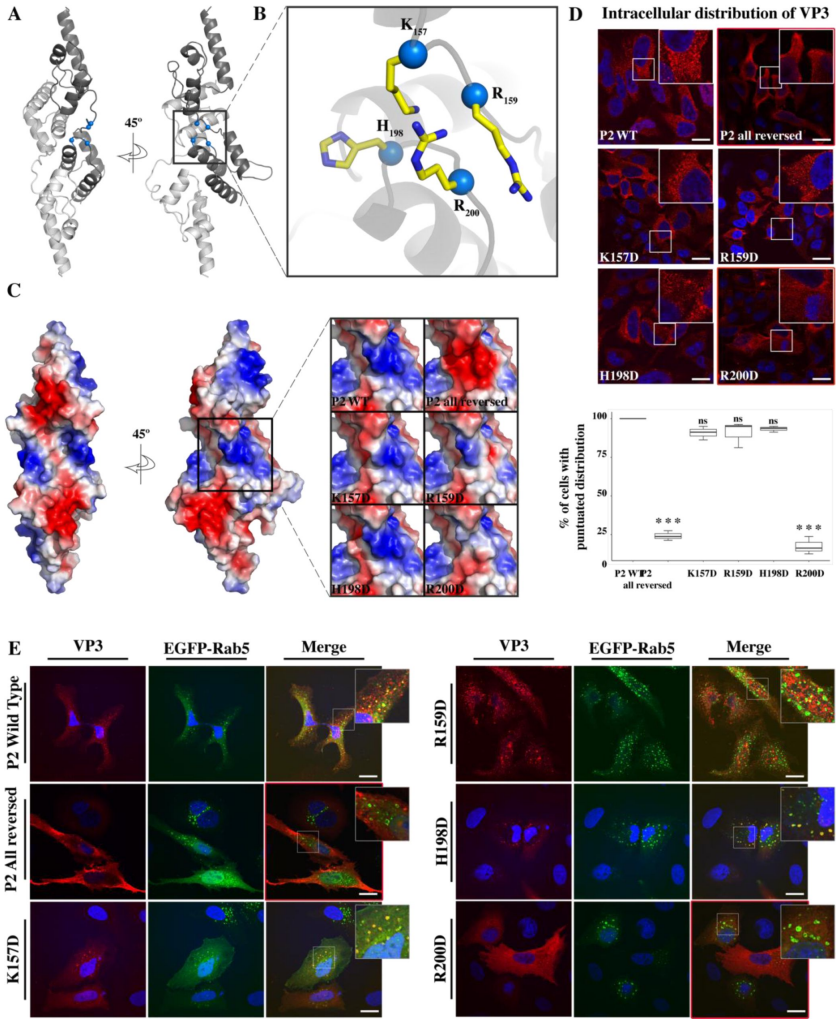

Figure 2.

VP3 P2 involvement in the association of VP3 with the EE membrane.

(A) The cartoon representation of the VP3 dimer [PDB 2R18 (Casañas et al., 2008)] shows each protomer in different shades of grey. The blue balls depict the residues defining the P2 region.
(B) The close-up of P2 region showing residues K_{157}, R_{159}, H_{198} and R_{200}.
(C) Electrostatic potential mapped on the surface of the structure of a VP3 dimer in the same orientations as in (A) structures. The close-up shows the impact of P2 residue mutations on the electrostatic potential of the binding site. P2 WT corresponds to the "UniProt code". The color-coded electrostatic surface potential of VP3 was drawn using PyMol (blue positive, red negative).
(D) QM7 cells transfected with pcDNA VP3 FL (P2 WT), P2 (all reversed), or the four point mutants ($K_{157}D$, $R_{159}D$, $H_{198}D$ and $R_{200}D$) and immunostained with anti-VP3 showing the distribution of each protein (upper panel). Images were captured using a Confocal Laser Scanning Microscopy and then the percentage of cells with punctated fluorescent signal were determined for each protein (lower panel). The red signal shows the VP3 distribution and the blue one shows the nuclei, which were Hoestch-stained. The data were normalized to the P2 WT protein. The box plot represents the percentage of cells with punctuated distribution of VP3. Significant differences (*** P <0.001; ns P >0.05.) as determined by one-way ANOVA with Tukey's HSD test.
(E) QM7 cells co-transfected with pEGFP-Rab5 and pcDNA VP3 FL (P2 WT), P2 (all reversed), or the four point mutants ($K_{157}D$, $R_{159}D$, $H_{198}D$ and $R_{200}D$) and immunostained with anti-VP3 showing the distribution of each protein. Representative images, captured using a Confocal Laser Scanning Microscopy are shown where green signal represents Rab5 distribution and the red signal that of VP3. Nuclei were Hoestch-stained and are blue. White bar-scales represent 20 µm. VP3 P2 (all reversed) and $R_{200}D$ depict a cytosolic distribution of the proteins. Quantification of the co-localization of the different VP3 proteins and EGFP-Rab5 is shown in *SI Appendix*, Fig. S3.

with a fluorescent anti-GST antibody. As an additional control in these experiments, we immunostained the EE with antibodies anti-EEA1. As shown in **Fig. 3B**, VP3 P2 WT demonstrated a conspicuous PI3P-bearing EEA1 positive endosomes location. In addition, we observed a similar distribution for VP3 K_{157D}, $R_{159}D$, and $H_{198}D$ and a drastic change in VP3 FL $R_{200}D$ mutant, which appeared utterly cytosolic, losing its capacity to bind to PI3P-bearing EE membranes (**Fig. 3B, red framed panel on the lowest row**). These results further support the role of R_{200} in this interaction.

VP3 R_{200} is crucial for binding to PI3P

To validate this, we devised a liposome co-flotation assay using a recombinant His-VP3 FL $R_{200}D$ mutant. When assayed in parallel with His-2xFYVE, we observed that His-VP3 FL $R_{200}D$ lost binding to PI3P(+) liposomes (**Fig. 4A**). To confirm that the lack of binding was not due to misfolding of the mutant, we compared the circular dichroism spectra of His-VP3 FL and His-VP3 FL $R_{200}D$ proteins, without detecting significant differences (**Fig. 4B**). To assess its relevance in IBDV infectivity, we resorted to an IBDV reverse genetics system, based on a modification of the system described by Qi and coworkers (Qi et al., 2007). The full length sequences of the IBDV RNA segments A and B, flanked by a hammerhead ribozyme at the 5'-end and the hepatitis delta ribozyme at the 3'-end, were expressed under the control of an RNA polymerase II promoter within the plasmids pCAGEN.Hmz.SegA.Hdz (SegA) and pCAGEN.Hmz.SegB.Hdz (SegB). For this specific experiment we generated a third plasmid, pCAGEN.Hmz.SegA.R_{200}D.Hdz (SegA.R_{200}D), harboring a mutant version of segment A cDNA containing the $R_{200}D$ substitution. Then, QM7 cells were transfected with the plasmids SegA, SegB or Seg.R_{200}D alone (as controls) or with a mixture of plasmids SegA+SegB (wild type situation) or SegA.R_{200}D+SegB (mutant situation). At 8 h post transfection (p.t.), when the new viruses have been able to assemble out of the two segments of RNA, the cells were recovered and re-plated onto fresh non-transfected cells to reveal the presence of infective viruses. At 72 h post-plating, the generation of foci forming units (FFUs) was revealed by Coomassie staining. As expected, single-transfections of SegA, SegB or Seg.R_{200}D did not produce FFUs. As shown in **Fig. 4C**, the transfection of SegA+SegB produced detectable FFUs (the three circles in the upper panel) while no FFUs (the three circles in the lower panel) were detected after the transfection of SegA.R_{200}D+SegB (**Fig. 4C**). Given the relevance of VP3 R_{200}, we assessed its conservation among members of the *Birnaviridae* family. For this, a multiple sequence alignment of VP3 reference sequences was performed (*SI Appendix*, Fig. S4A). As shown, IBDV VP3 has 32-39% identity to the other selected homologues (*SI Appendix*, Fig. S4B). A closer look at the VP3 P2 revealed the complete conservation of R_{200} (**Fig. 4D**). Taken together, these findings show that VP3 R_{200} plays an important role mediating the VP3-PI3P interaction, highlighting the active participation of EE membranes during the infectious cycle of birnaviruses.

Electrostatic forces mediate VP3 membrane binding

Computer simulations based on coarse-grain models were performed to assess the binding free-energy and adsorption mechanism of three protein variants: VP3 Ct, VP3 ΔNt, and VP3 FL. The VP3 Ct region, with a positive electrical charge of +5, was modeled as an intrinsically disordered region according to the AlphaFold2 prediction (**Fig. 1E**). VP3 ΔNt encompasses residues 82 to 257 and is electroneutral. This variant was chosen primarily because it retains the structural data from the crystallized protein. Similarly to His-VP3 FL, His-VP3 ΔNt retains the ability to bind to liposomes PI3P(+) (see *SI Appendix*, Fig. S5). Finally, VP3 FL is the full length monomeric VP3, using the AlphaFold2 predicted structure with an overall electrostatic charge of -3. We employed the Molecular Theory (MT) approach to obtain adsorption free-energy profiles, PMF(z), at different salt concentrations (Chiarpotti et al., 2021; Ramírez et al., 2019). The membrane was modeled as a rigid dielectric slab with 5% of its surface occupied by ternary ionizable groups. **Figure 5** (panels A-C) shows the PMF(z), where z represents the distance between the center of mass of the protein and the center of the membrane, at 50 and 150 mM NaCl. As observed in **Fig. 5A**, the

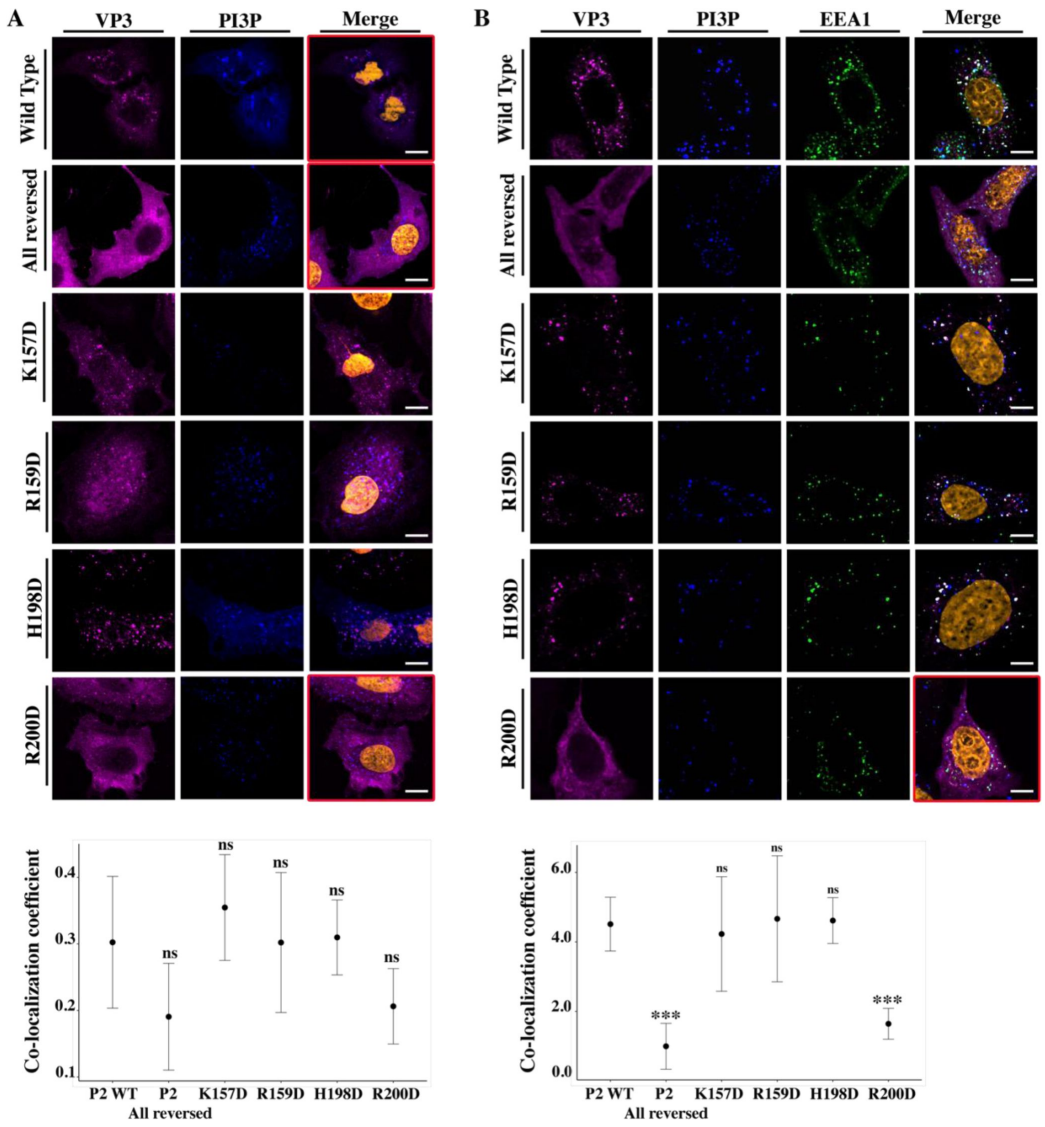

Figure 3.

VP3 P2 involvement in the association between VP3 and EE PI3P.

(A) QM7 cells co-transfected with the PI3P biosensor pEGFP-2xFYVE and pcDNA VP3 FL (P2 WT), P2 (all reversed), or the four point mutants ($K_{157}D$, $R_{159}D$, $H_{198}D$ and $R_{200}D$) and immunostained with anti-VP3 showing the distribution of each protein. Representative images captured using a Confocal Laser Scanning Microscopy are shown where blue signal represents FYVE distribution and the magenta signal that of VP3. Nuclei were Hoestch-stained and are orange (upper panels). White bar-scales represent 20 µm. VP3 P2 (all reversed) and $R_{200}D$ depict a cytosolic distribution of the proteins with a significant lower co-localization coefficient. The dot plot in the lower panel depicts the co-localization coefficient for each protein determined as explained in the Materials and Methods section. Significant differences (ns P >0.05) as determined by one-way ANOVA with Tukey's HSD test.

(B) QM7 cells were transfected with the pcDNA VP3 FL (P2 WT), P2 (all reversed), or the four point mutants ($K_{157}D$, $R_{159}D$, $H_{198}D$ and $R_{200}D$). The cells were fixed and then the GST-2xFYVE purified peptide and anti-VP3 antibodies were used to recognize endogenous PI3P and VP3, respectively. Additionally anti-EEA1 antibodies were used to stain the endosomes. GST-2xFYVE was labelled with a fluorescent anti-GST antibody (blue signal), anti-VP3 and anti-EEA1 antibodies with fluorescent secondary antibodies (magenta and green signals, respectively), and Hoestch-stained nuclei in orange. White bar-scales represent 10 µm. VP3 P2 (all reversed) and $R_{200}D$ depict a cytosolic distribution of the proteins with a significant lower co-localization coefficient. The dot plot in the lower panel depicts the co-localization coefficient for each protein determined as explained in the Materials and Methods section. Significant differences (*** P < 0.001; ns P >0.05) as determined by one-way ANOVA with Tukey's HSD test.

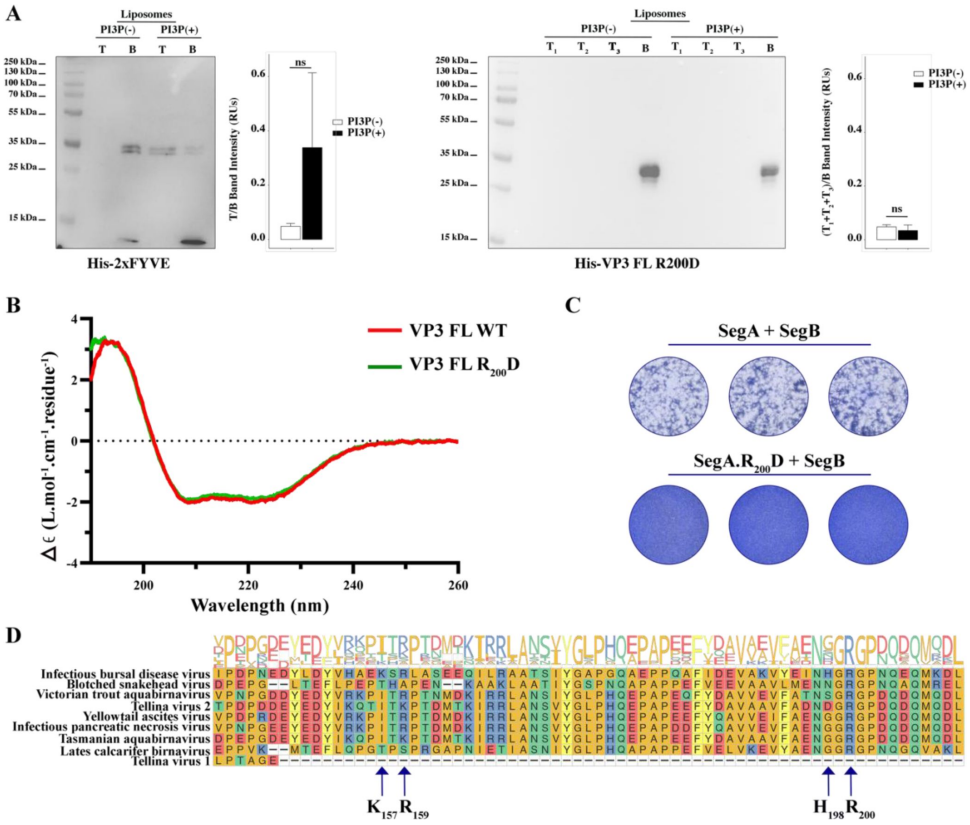

Figure 4.

Biophysical characterization of VP3 FL $R_{200}D$ binding to PI3P.

(A, left panel). Immunoblots of the top (T) and bottom (B) fractions from a liposome PI3P(-) or PI3P(+) OptiprepTM co-floatation assay indicating that His-2xFYVE protein (~35 kDa) specifically binds to liposome PI3P(+). The bar plot represents the intensity of T/B bands for each liposome preparation. Significant differences (ns P >0.05) as determined by one-way ANOVA with Tukey's HSD test.

(A, rigth panel). Immunoblots of the three top (T_1, T_2 and T_3) and bottom (B) fractions from a liposome PI3P(-) or PI3P(+) OptiprepTM co-floatation assay indicating that His-VP3 FL $R_{200}D$ protein (~35 kDa) does not bind to liposome PI3P(-) nor PI3P(+). The bar plot represents the intensity of (T_1+T_2+T_3)/B bands for each liposome preparation. Significant differences (ns P >0.05) as determined by one-way ANOVA with Tukey's HSD test.

(B) Far-UV CD spectra of His-VP3 FL (red line) or His-VP3 FL $R_{200}D$ (green line). Spectral acquisitions at 50 nm/min with 0.1 nm steps at 1 s integration time, with a bandwidth of 1 nm were performed 4 times for the samples as well as for the buffer. The measurements were carried out with constant nitrogen gas flux of 10 ml/min. Acquisitions were averaged and buffer baseline was subtracted with Spectra Manager (JASCO). No smoothing was applied. CDtoolX was used to zero between 255-260 nm and to calibrate the signal amplitude from the fresh CSA signal (Miles and Wallace, 2018). Data are presented as delta epsilon (Δε) per residue (L.mol-^{1}.cm-^{1}.residue^1) calculated using the molar concentration of protein and number of residues.

(C) QM7 cells were grown in M24 multi-well plate for 12 h to approximately 90-95% confluency and then 800 ng of plasmids were transfected [(SegA + SegB) or (SegA.$R_{200}D$ + SegB)] in triplicate. At 8 h post-transfection (p.t.) the supernatants were discarded, and the monolayers were recovered for further plating on M6 multi-well plates containing non transfected QM7 cells. Avicel RC-591 (FMC Biopolymer) was added to the M6 multi-well plates. 72 h p.i., the monolayers were fixated and stained with Coomassie R250 for revealing the foci forming units.

(D) Partial view of amino acid alignment of the VP3 protein for nine reference members of *Birnaviridae* family. Multiple sequence alignment was performed with Clustal OMEGA (v1.2.4) (Sievers et al., 2011) implemented at EMBL's European Bioinformatics Institute ("EMBL's European Bioinformatics Institute," n.d.) (The complete alignment is shown in *SI Appendix,* Fig. S4A). Alignment visualization was done with the R *ggmsa* package (Zhou et al., 2022) in with assistance from the RStudio software (RStudio Team, 2020). Amino acids are colored according to their side-chain chemistry. Protein sequence logos annotation is displayed on top of the amino acid alignment. For facilitating the view IBDV VP3 142-210 portion is shown. The black arrow indicates the K_{157}, R_{159}, H_{198} and R_{200}.

positively charged VP3 Ct shows the highest affinity for the membrane due to the deprotonation of the acidic lipids at pH 8, resulting in a net negative charge on the membrane surface (*SI Appendix*, Fig. S6). However, the electroneutral construct VP3 ΔNt has a lower binding energy than VP3 Ct, and also VP3 FL shows some degree of membrane binding, despite both the protein and the membrane being negatively charged, as evidenced by the shallow minimum in the PMF.

The binding of the three protein constructs was strongly affected by electrostatics, as shown in **Fig. 5D**, where the adsorption energy is plotted as a function of the concentration of salt. The effect of salt concentration is most significant for VP3 Ct, but it is also noticeable for VP3 ΔNt and VP3 FL. Also, the interfacial concentration of each construct was higher at lower ionic strengths, as depicted in *SI Appendix*, Fig. S7. The weak binding energy of VP3 FL to the anionic membrane under physiological conditions (~150 mM NaCl, pH 7) was consistent with the experimental observation that VP3 FL did not bind to liposomes PA and PI, which are anionic at the pH of the experiments. However, those same experiments showed that VP3 FL did bind to PI3P(+) liposomes (**Fig. 1B-C**), despite the MT calculations predicting weak binding. Taken together, our results suggest that specific VP3-PI3P interactions enhance the binding of VP3 to PI3P-containing EE membranes, while exhibiting weak and non-specific electrostatic attractions to an otherwise generic anionic membrane. *SI Appendix*, Fig. S8 illustrates the distribution of cationic residues of VP3 near the membrane, indicating that the Ct fragment drives the non-specific binding. To identify the electrical charge of different protein regions, *SI Appendix* Fig. S9 shows a map of the electrostatic potential around VP3 FL.

Molecular Dynamics (MD) simulations based on the MARTINI model were employed to further investigate the mechanism by which VP3 Ct and VP3 ΔNt approach the membrane surface. We chose VP3 ΔNt over VP3 FL because VP3 ΔNt has a closer resemblance to the well-established experimental crystal structure. Additionally, the adsorption free energy profiles predicted by MT for both VP3 ΔNt and VP3 FL are notably similar (compare panels B and C of **Figure 5**). Unlike the MT model, MARTINI considers both electrostatic and van der Waals forces (De Jong et al., 2013). To mimic the liposome PI3P(+) composition used in the co-flotation assays, the lipid bilayer was modeled with a molar ratio of 64:31:5 for the lipids DOPE, DOPC, and PI3P, respectively. DOPE and DOPC are electroneutral, PI3P is anionic. The MD simulations revealed that both VP3 Ct and VP3 ΔNt settled on the membrane surface after 120 ns, as shown in *SI Appendix*, Fig. S10. **Figure 6A-D** shows a temporal sequence of configurations during the adsorption of VP3 ΔNt. The protein approached the membrane via the Ct fragment and remained adsorbed during the rest of the 500 ns trajectory. VP3 Ct exhibited the same behavior, as demonstrated in *SI Appendix*, Fig. S10 and Fig. S11. Notably, VP3 Ct and VP3 ΔNt did not detach from the surface during these MD simulations, suggesting that the adsorption energies calculated by MT were underestimated and represent a lower bound, as van der Waals interactions are absent in the MT model. Also, **Fig. 6E** highlights the location of the four positive residues that make up the P2 region, showing their proximity to the membrane surface.

Recruitment of PI3P modulates the membrane binding of VP3

We investigated the impact of VP3 Ct and VP3 ΔNt on the composition of the membrane near the binding point, and on the local curvature of PI3P(+) liposomes. We resorted to our MD simulations and evaluated the in-plane radial distribution function, g(r), between the center of mass of the proteins and the center of mass of PI3P molecules in the (cis) hemilayer, which is in direct contact with the protein. **Figure 6F** shows that VP3 Ct recruits PI3P within a ~2 nm radius, where its local concentration in the cis hemilayer is up to 6 times greater than the average PI3P concentration (*SI Appendix*, Fig. S12). Also, despite having no net electrical charge, VP3 ΔNt induces a similar concentration enhancement, with PI3P accumulation occurring around the Ct fragment, as evidenced in *SI Appendix*, Fig. S13. In both cases, the recruitment of PI3P in the cis hemilayer is accompanied by a local depletion of PI3P in the trans hemilayer, due to interhemilayer electrostatic repulsions. The effects on PI3P concentration, induced by VP3 ΔNt, result from a

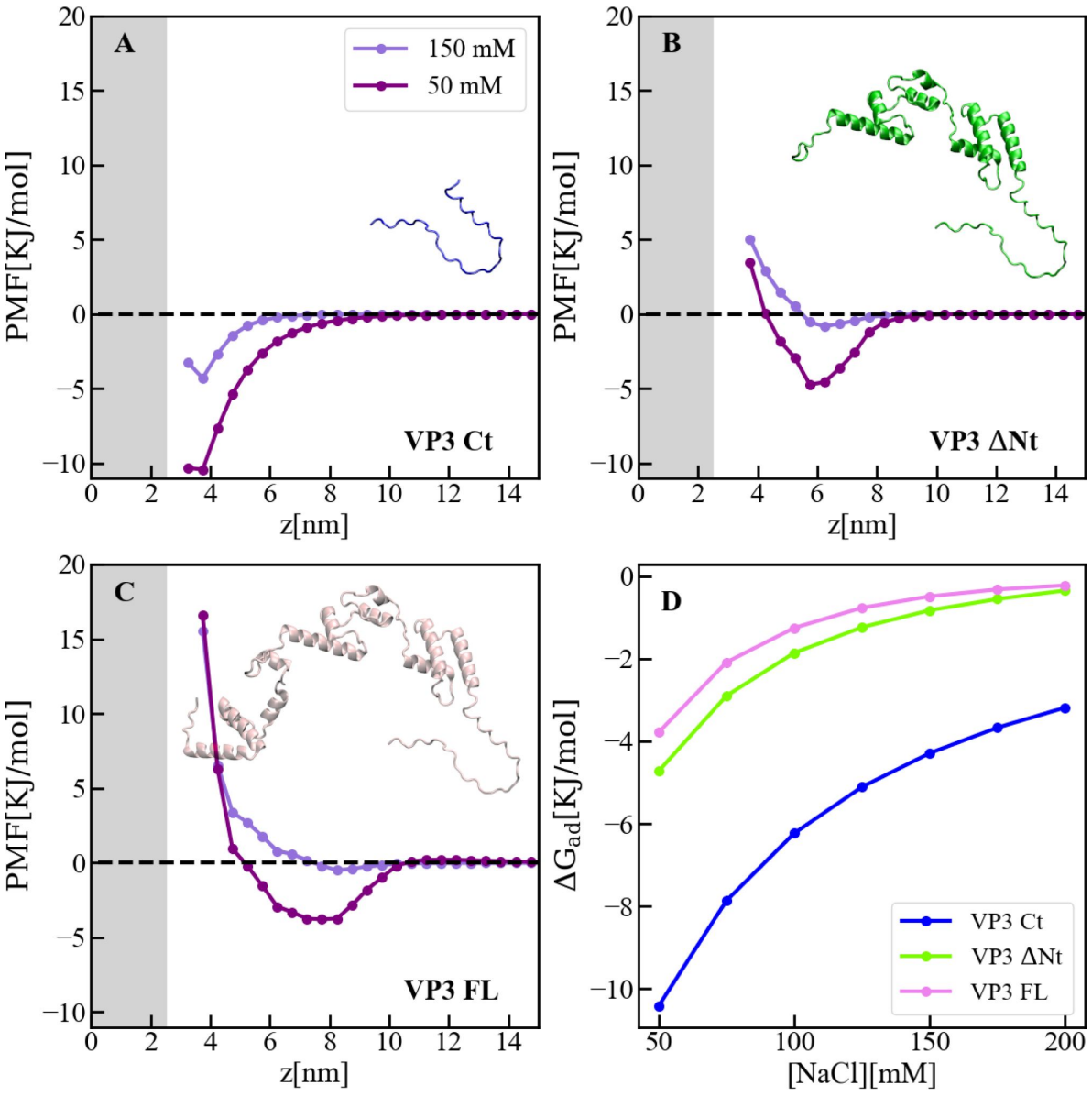

Figure 5.

Adsorption of VP3 constructs to PI3P(+) model membranes.

(A-C). Adsorption free-energy profiles, PMF(z),for VP3 Ct, VP3 ΔNt and VP3 FL at 50 and 150 mM of NaCl.
(D) Adsorption free energy (ΔG_{ad}), computed from the minimum of PMF(z), versus concentration of NaCl. In all cases, the solution pH is 8, and the concentration of protein is 1 μM. The grey areas represent the volume excluded by half the membrane (cis hemilayer, z>0). The membrane surface contains 5% titratable groups, representing PI3P. Each group has three acidic moieties, one with a pKa of 2.5 and the others with 6.5. At 150 mM NaCl and pH 8, more than 90% of the acidic groups are deprotonated (*SI Appendix*, Fig. S5).

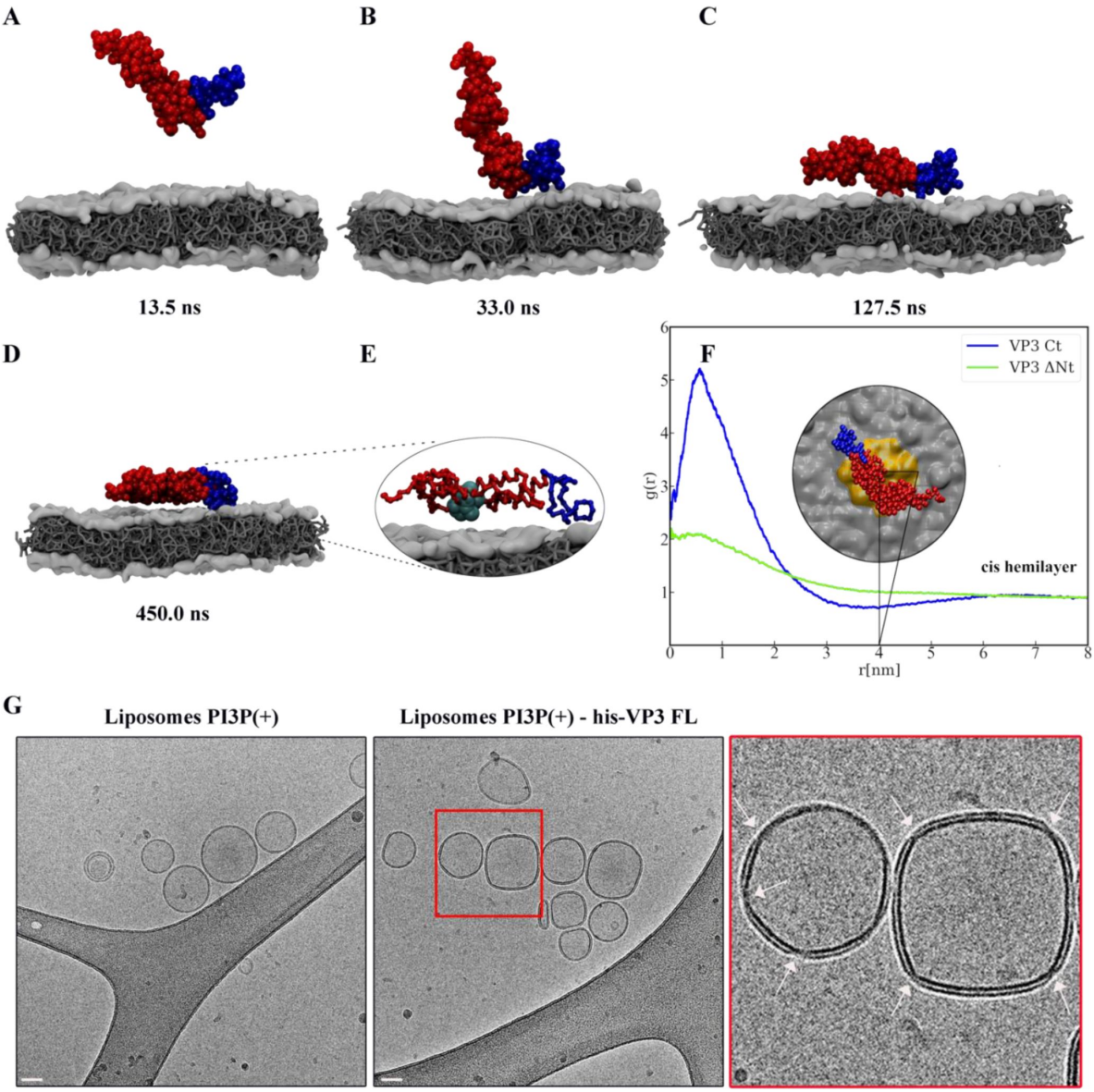

Figure 6.

VP3 approaching a lipid bilayer, and distortion of the membrane.

(A-D) Temporal sequence of configurations illustrating how VP3 DNt approaches the negatively charged membrane during a 500 ns MD simulation. The membrane contains DOPE, DOPC and PI3P in 64:31:5 molar ratio. The beads making the Ct fragment are colored blue.
(E) Magnification of the protein configuration bound to the membrane, with P2 residues represented in cyan balls.
(F) Radial distribution function, g(r), between the center of mass of VP3 DNt and the center of PI3P molecules in the cis hemilayer. g(r) greater than 1 implies local enhancement of PI3P concentration. The inset shows an upper view of VP3 DNt bound to the membrane, with the area within r = 4 nm colored in orange.
(G) Cryo-electron microscopy images of cryo-fixated liposomes PI3P(+) control (without protein, left panel), or incubated with His-VP3 FL showing the small pinches or localized thinnings in the bilayer of the liposomes when His-VP3 FL was present (middle panel). The bar represents 50 nm. The right panel represents an enlarged image of the red square on the middle panel. White arrows point to the small pinches or localized thinnings in the bilayer when His-VP3 FL was present.

synergistic action between the positively charged Ct and the P2 region of the protein. Furthermore, when mutations are introduced to the P2 region - starting with $R_{200}D$ and eventually including the entire P2 domain - there is a gradual reduction in its contribution to the recruitment of PI3P (see *SI Appendix*, Fig. S14). Molecular Theory calculations on these mutants also reveal that the binding free energy of both VP3 ΔNt P2 Mut and VP3 ΔNt $R_{200}D$ is consistently lower than that of VP3 ΔNt across all salt concentrations explored (see SI Appendix, Fig. S15). This indicates a weakening of the interaction with the negatively charged membrane, concomitant with the loss of positively charged amino acids.

Finally, to examine the potential impact of VP3 on the lipid bilayer, we incubated liposomes PI3P(-) and PI3P(+) with purified His-VP3 FL as described previously. The samples were cryo-fixed and cryo-EM was used to observe the resulting structures. As shown in **Fig. 6G**, His-VP3 FL distorts the membrane of liposomes containing PI3P, resulting in small pinches in the bilayer, detectable in 36% of the liposomes PI3P(+), while it is completely absent in PI3P(-) liposomes. Taken together, our findings suggest that the binding of VP3 to EE membranes has the potential to alter the local lipid composition by recruiting PI3P, which could then lead to the localized membrane pinches observed in **Figure 6G**.

Discussion

Several viruses hijack the PI3P metabolism machinery to complete their infectious cycle. However, only a few cases of viral proteins that bind PI3P have been described. Equine infectious anemia virus (EIAV) is a member of the lentivirus subgroup of retroviruses and replicates in macrophages. Retroviral assembly and release are directed by the structural precursor polyprotein Gag (Wills and Craven, 1991). EIAV Gag localizes to both the cell interior and to the plasma membrane due to its high-affinity interaction with PI3P (Fernandes et al., 2011; Puffer et al., 1998; Tanzi et al., 2003). Moreover, mutation of K_{49}, a residue in the PIs-binding pocket of Gag inhibited the release of viral-like particles from the plasma membrane (Fernandes et al., 2011). Another example are the poxviruses, a family of cytoplasmic DNA viruses that also rely on intracellular membranes to develop their envelope, whose morphogenesis requires enzymes from the cellular phosphoinositide metabolic pathway (Mcnulty et al., 2010). For vaccinia virus (VACV), the prototypic poxvirus, Kolli and coworkers showed that the VACV H7 protein binds to PI3P and PI4P (Kolli et al., 2015). Similarly to our observations in IBDV VP3, the authors uncovered two regions of H7 essential for viral replication. One region is a positive surface patch centered on K_{108}, and the other region is the flexible Ct tail (Kolli et al., 2015).

Our biophysical and molecular simulation results suggest a specific but weak interaction of VP3 with PI3P bearing membranes. In co-floatation assays, we observed that His-VP3 FL reaches the top of the gradient, where liposomes PI3P(+) are located, with a high proportion of protein still found at the bottom of the gradient. This phenomenon was not observed with the His-2xFYVE protein. Additionally, the slopes of the BLI curves show that His-VP3 FL dissociate faster than His-2xFYVE from liposomes PI3P(+). Computer simulations have also revealed a weak attractive interaction between the negatively charged VP3 and membranes that contain PI3P. VP3 bears multiple essential roles during the viral life cycle. In this context, our hypothesis is that an early, specific, but weak interaction with PI3P is required for the formation of RCs associated with EE and represents an advantage for the virus that counts with VP3 to go forward into the replication cycle.

We identified the domain of VP3 involved in PI3P-binding, and established the critical role played by the arginine residue at position 200 of VP3 (R_{200}). This arginine is conserved among all known birnaviruses. Mutating R_{200} abolishes viral replication. As previously mentioned, VP3 is a multifunctional viral protein. Therefore, it was initially possible that mutating R_{200} might affect other functions beyond PI3P binding and viral replication. However, R_{200} is not located in any of

the protein regions associated with its other known functions. For instance, the VP3 dimerization domain, located in the second helical domain, involves 81 interprotomeric contacts across three helices, but R_{200} does not participate in these contacts (Casañas et al., 2008). Also, VP3 has an oligomerization domain mapped within the 42 C-terminal residues of the polypeptide, i.e., the segment of the protein composed by the residues at positions 216-257 (Maraver et al., 2003); VP3's ability to bind RNA is facilitated by a region of positively-charged amino acids, identified as P1, which includes K_{99}, R_{102}, K_{105}, and K_{106} (Valli et al., 2012). Furthermore, our findings indicate that the R_{200}D mutant retains a folding pattern similar to the wild-type protein. All these lead us to conclude that the loss of replication capacity of R_{200}D viruses results from impaired, or even loss of, VP3-PI3P interaction.

It has recently been reported that the RCs of IBDV exhibit liquid-liquid phase separation (LLPS) (Reddy et al., 2022). In LLPS, one or more biomolecules form a network of mild homo- and heterotypic interactions, resulting in the formation of a distinct liquid phase within a liquid medium (Banani et al., 2017). In light of our results, it is conceivable to hypothesize that viral interaction with the EE membranes acts as a first step in the RCs biogenesis, leading to the growth of biomolecular condensates with LLPS characteristics around EE membranes, as recently proposed (Brodrick and Broadbent, 2023). In support of this model, both the RNA dependent RNA polymerase VP1 and the viral dsRNA associate to endosomes and to the LLPS condensates (Delgui et al., 2013; Reddy et al., 2022). Further experiments are needed in order to link the association of VP3 to EE membranes with biomolecular condensate formation.

Evolutionary links between +sRNA and dsRNA viruses

Birnaviruses integrate the double-strand RNA Baltimore group (Baltimore, 1971), and the newly created *Riboviria* taxon (a realm), that includes all RNA viruses encoding RdRps (Walker et al., 2021). However, the organization of the birnaviral RdRp (Gorbalenya et al., 2002) and the structure of its capsid (Coulibaly et al., 2005) had already indicated strong links between birnaviruses and +sRNA viruses, placing them in a special branch of the dsRNA viruses that appears to have evolved independently of the others. The membrane association of their replication complexes is a further specificity of birnaviruses that links them more to the +sRNA viruses than to the other dsRNA viruses. Indeed, within the megataxonomy merging together Baltimoreś and Linnean classifications proposed by Koonin *et al*., the *Birnaviridae* family status is uncertain (Koonin et al., 2020).

Materials and methods

Recombinant prokaryotic-expression plasmid

We used an *Escherichia coli*-based prokaryotic system to obtain the His-2xFYVE and GST-2xFYVE fusion proteins. For the first one, the plasmid encoding EGFP-2xFYVE, pEGFP-2xFYVE, generated by Gillooly and collaborators (Gillooly et al., 2000) was kindly provided by Harald A. Stenmark (Norwegian Radium Hospital, Oslo, Norway) to our group and used as a template. The 2xFYVE fingers consisted in duplicated domains of residues 147-223 of mouse hepatocyte growth factor-regulated tyrosine kinase substrate (Hrs) (Komada and Kitamura, 1995) separated by a QGQGS linker. The prokaryotic vector expressing 2xFYVE was obtained following standard PCR methods with the oligonucleotide pair 2xFYVE (*SI Appendix*, Table 1). The PCR fragment was inserted into the pET32a(+), which incorporates the thioredoxin A (TrxA) gene, a 6xHis tag and Thrombin site (Ts) within the amino-terminal domain of the 2xFYVE, and the correctness of the insertion was confirmed by sequencing. The complete fusion protein TrxA.His.Ts.2xFYVE (hereafter named His-2xFYVE) is 954 base pairs (bp)-long and contains 317 residues (~35 kDa). The plasmid encoding GST-2xFYVE was kindly gifted by Harald A. Stenmark (Norwegian Radium Hospital, Oslo, Norway) to the group of Etienne Morel.

Recombinant eukaryotic-expression plasmids

We used a *Baculovirus*-based eukaryotic system to obtain the His-VP3 FL, His-VP3 FL $R_{200}D$ and His-VP3 ΔCt fusion proteins. The construct of the recombinant baculovirus (rBV) His-VP3 FL was generated from IBDV VP3 FL protein [strain Soroa, GenBank AF140705.1, residues 756-1012 (257 residues) from the polyprotein] cloned in pcDNA vector. Thus, IBDV VP3 FL protein was subcloned from plasmid pcDNA VP3 FL into the pFast Bac HTb vector (Gibco BRL), which incorporates a 6xHis tag at the N-terminal of the recombinant protein. Briefly, VP3 FL coding sequence was amplified by PCR with the oligonucleotide pairs VP3.Fw and VP3.Rv incorporating *Bam*HI and *Eco*RI restriction sites, respectively (*SI Appendix*, Table 1). The resulting DNA fragment containing the VP3 gene was digested with *Bam*HI and *Eco*RI and ligated to plasmid pFast Bac HTb restricted with the same enzymes, generating the plasmid pFast Bac-his-VP3 FL. This plasmid contained the VP3 gene fused to a histidine tag under the control of the polyhedrin promoter. The complete fusion protein His-VP3 FL is 861 bp-long and contains 286 residues (~32 kDa). The generation of rBV His-VP3 FL $R_{200}D$ was performed following the same procedure, but using the pcDNAVP3 FL $R_{200}D$ as a template for subcloning. The complete fusion protein His-VP3 FL $R_{200}D$ is 861 bp-long and contains 286 residues (~32 kDa). The generation of rBV His-VP3 Δ223-257 (His-VP3 ΔCt) was performed as follows. A 663 nucleotide DNA fragment containing a truncated version of the VP3 sequence encoding a polypeptide lacking the 36 carboxi-terminal residues was amplified by PCR from pcDNAVP3 FL with the oligonucleotide pairs VP3.Fw and VP3 Δ223-257.Rv incorporating *Bam*HI and *Eco*RI restriction sites, respectively (*SI Appendix*, Table 1). The DNA fragment was digested with *Bam*HI and *Eco*RI and was ligated to plasmid pFast Bac HTb restricted with the same enzymes, generating the plasmid pFast Bac-his-VP3 Δ223-257, hereafter named His-VP3 ΔCt. All the resulting plasmids were subjected to nucleotide sequencing to assess the correctness of the inserted VP3 sequence, and they were then used to produce the corresponding rBVs by using the Bac-to-Bac system and by following the manufacturer's instructions (Invitrogen). Briefly, the recombinant plasmids were transformed into DH10Bac competent cells to obtain recombinant bacmids. The white colonies on culture plates were picked, confirmed by PCR and used for Sf9 cell transfection by using Cellfectin II Reagent (Gibco). The transfected cells were cultured at 28°C for 5 days to produce rBVs. Then, the cells were subjected to Western blot analysis for recombinant proteins expression confirmation and the supernatant (P1) was used to amplify the rBVs to a higher-titre P2 and scaled up to obtain a higher volume of P3 to be titrated (Plate-Forme Technologique Production et Purification de Protéines Recombinantes, Institut Pasteur) and used for protein production.

Protein expression and purification

His-VP3 polypeptides were produced in the Bac-to-Bac™ Baculovirus Expression System. Briefly, Sf9 cells (Gibco, ThermoFisher Scientific) were infected with recombinant Baculoviruses (rBVs) at a multiplicity of infection (MOI) of 5 PFU/cell. Cells were harvested at 96 h post-infection, washed once with chilled phosphate-buffered saline (PBS), resuspended in lysis buffer [50 mM Tris-HCl (pH 8.0), 500 mM NaCl, 0.1% nonidet P-40) supplemented with protease inhibitors (Complete Mini, Roche), and maintained on ice for 30 min. Thereafter, extracts were sonicated and centrifuged at 13.000 g for 15 min at 4°C. Supernatants were collected and subjected to immobilized metal-affinity chromatography (IMAC) purification by using a Ni^{2+} affinity column (HiTrap Fast Flow Crude, GE Healthcare). Resin-bound proteins were eluted with elution buffer [50 mM Tris-HCl (pH 8.0), 500 mM NaCl, 500 mM imidazole]. His-tagged VP3 FL, VP3 ΔCt or VP3 FL $R_{200}D$ -containing fractions were pooled and subjected to size exclusion chromatography using a Superdex 200 column (GE HealthCare). Finally, protein samples were concentrated to a final concentration of ~3 mg/ml by using Centricon filters (Millipore), aliquoted and flash-frozen in liquid nitrogen for -80°C storage. The His-VP3 FL, His-VP3 ΔCt and His-VP3 FL $R_{200}D$ fusion proteins obtained from Baculoviruses were used for co-flotation, bio-layer interferometry and cryo-EM assays.

For His-2xFYVE polypeptide production, *E. coli* BL21 DE3 cells containing the plasmid pET32a(+)-2xFYVE were grown at 37°C until an OD600 of 0.6 was reached. Protein expression was induced overnight at 18°C using 1mM IPTG. Cells were harvested via centrifugation, resuspended in buffer [10 mM TRIS-HCl (pH 8.0), 100 mM NaCl] supplemented with protease inhibitors and sonicated. The cell lysate was clarified via centrifugation at 18.000 g for 20 min at 4°C and the resulting supernatant was subjected to IMAC purification by using a Ni^{2+} affinity column (HiTrap Fast Flow Crude, GE Healthcare). Resin-bound proteins were eluted with elution buffer [10 mM TRIS-HCl (pH 8.0), 100 mM NaCl, 500 mM imidazole]. His-2xFYVE-containing fractions were pooled and subjected to size exclusion chromatography using a Superdex 75 column (GE HealthCare). Finally, protein samples were concentrated to a final concentration of ~3 mg/ml by using Centricon filters (Millipore), aliquoted and flash-frozen in liquid nitrogen for -80°C storage. The His-2xFYVE was used as a positive control in co-flotation, bio-layer interferometry and cryo-EM assays.

For GST-2xFYVE polypeptide production, a classical GST fusion protein purification protocol, using pGEX-5X-1 vector (GE Healthcare, 27-4584-01) cloning as described was followed (Nascimbeni et al., 2017). Briefly, *E. coli* BL21 DE3 strain maxi-cultures were lysed and subjected to glutathione beads binding for GST purification. The glutathione beads were finally treated with benzamidine-coated beads (GE Healthcare Life Science, 17512301) to remove the factor Xa and dialyzed for the final purification in a 75 mM Kac, 30 mM HEPES, pH 7.4, 5 mM $MgCl_2$ solution. The GST-2xFYVE fusion protein was used as a probe to detect PI3P in immunofluorescence assays.

Purified proteins quantification and quality control assessment

His-VP3 FL, VP3 ΔCt, VP3 FL $R_{200}D$, and His-2xFYVE quantification at 280 nm was carried out by recording a full spectrum between 240 and 340 nm. Measurements were done with 60 µL of buffer and sample at 20°C in a 1 cm quartz cell, reference 105.202-QS.10 (Hellma Analytics, France), using a JASCO V-750 spectrophotometer (JASCO Corporation, Japan). A baseline subtraction at 340 nm was performed with the Spectragryph software to accurately calculate the protein concentration. The assessment of the sample homogeneity was performed by Dynamic Light Scattering (DLS) analysis on a DynaPro Plate Reader III (Wyatt, Santa Barbara, CA, USA) to ensure that the samples did not contain aggregates. A volume of 20 µL of sample was loaded in a 384-well microplate (Corning ref 3540, New-York, USA), with 10 acquisitions of 5 s each at 20°C, monitored with the DYNAMICS version V7.10.0.21 software (Wyatt, Santa Barbara, CA, USA), three repetitions per measurement. Finally, the protein integrity and purity were assessed by intact mass spectrometry on a Bruker UltrafeXtreme MALDI-TOF/TOF instrument. A volume of 15 µL of protein was passed through a ZipTip C4 and eluted on a MTP 384 ground steel target plate (Bruker-Daltonics, Germany) with 2 µl of a 20 mg/ml α-Cyano-4-hydroxycinnamic acid in 50% acetonitrile, 0.1% trifluoroacetic acid as matrix solution. Data were acquired using Flexcontrol software (Bruker-Daltonics, Germany) and shots were recorded in positive ion linear mode. Mass spectra were externally calibrated in the m/z range of 15-60 kDa with the Protein II (Bruker-Daltonics, Germany) and analyzed with the flexAnalysis software (Bruker).

Liposome preparation

Liposomes were freshly prepared by the freeze-thaw and extrusion method (F Olson, C A Hunt and W J Vail, 1979). Briefly, lipids dissolved in chloroform were mixed and placed in glass vials, and the chloroform was evaporated by centrifuging 2 h at 35°C in a SpeedVac. The dried lipids were resuspended in a binding buffer composed of 150 mM NaCl, 20 mM Tris-HCl, pH 8 to a final concentration of 5 mM. The preparation was submitted to ten cycles of freezing in liquid nitrogen and thawing in a 37°C water bath. To generate small unilamellar liposomes, the multilamellar lipids were extruded through polycarbonate membranes (pore size 200 nm, Whatman). The liposomes were used within 1 week. The lipids POPE (1-palmitoyl-2-oleoyl-sn-glycero-3-phosphoethanolamine), POPC (1-palmitoyl-2-oleoyl-sn-glycero-3-phosphocholine), PI3P [1,2-dioleoyl-sn-glycero-3-phospho'(1'-myo-inosito'-3'-phosphate)], PA (1,2-dioleoyl-sn-glycero-3-

phosphate) and PI [1,2-dioleoyl-sn-glycero-3-phospho'(1'-myo-inositol)] were purchased from Avanti Polar Lipids. Liposomes PI3P(-) liposomes were prepared as a mixture of POPE and POPC at a molar ratio of 64:36. Liposomes PI3P(+), PA(+) or PI(+) were prepared as a mixture of POPE and POPC, with either PI3P, PA or PI at a molar ratio of 64:31:5.

Liposome co-flotation assay

For liposome co-flotation assays, the following proteins were used: His-VP3 FL, VP3 ΔCt, VP3 FL $R_{200}D$ produced in the Bac-to-Bac™ Baculovirus Expression System (Invitrogen), and His-2xFYVE produced using the *Escherichia coli* prokaryotic system. Then, 3 mM liposomes were incubated with 1 µM protein in binding buffer composed of 150 mM NaCl, 20 mM Tris-HCl, pH 8 at 4°C overnight (on), in a final volume of 100 µl. Liposomes and liposome-protein complexes were separated from unbound protein by ultracentrifugation of the reaction mixture in 5 mL Optiprep™ (Axis-Shield PoC AS) density gradients for 1 hour at 40,000 ×g (SW55Ti Beckman Coulter rotor). The liposome-protein mixture was adjusted to 34% Optiprep concentration in a volume of 300 µl, and loaded onto the bottom of the tube that contained 4.5 ml of 20% Optiprep in 150 mM NaCl, 20 mM Tris-HCl, pH 8, overlaid with 200 µl of the buffer. The three top and the bottom fractions, containing 400 µl of the gradient were used for SDS-PAGE gel analysis and immunoblotting against His-tag and anti-VP3 rabbit polyclonal serum.

Cryo-electron microscopy

Protein-liposome complexes were prepared as described for co-flotation assays. Then, 4 µl of the samples were spotted on glow-discharged lacey grids (S166-3, EMS) and cryo-fixed by plunge freezing at -180°C in liquid ethane using a Leica EMGP (Leica, Austria). Grids were observed with a Tecnai F20 electron microscope (Thermo Fisher Scientific). The Tecnai F20 was operated at 200 kV and images were acquired under low-dose conditions using the software EPU (Thermo Fisher Scientific) and a direct detector Falcon II (Thermo Fisher Scientific). For immunogold staining, the purified protein were first incubated with 5 µL of Ni-NTA [nickel (II) nitrilotriacetic acid] gold particles 0.5 mM in a five times gold particles/purified protein proportion in binding buffer to a final volume of 10 µl. This reagent comprises 5 nm gold particles covered with multiple Ni-NTA functionalities incorporated into the ligands on the surface of gold particles. Each Ni^{2+} coordinates with one NTA and two histidines from the His-tagged recombinant protein to form a stable complex with extremely low dissociation constants (Reddy et al., 2005). Then, 4 µl of this mix were incubated with 6 µl of 3 mM liposome preparation on at 4°C. Finally, 4 µl of each complex was subjected to cryo-fixation and cryo-EM analyzed as mentioned.

Bio-layer interferometry (BLI) assays

His-2xFYVE, His-VP3 FL or His-VP3 ΔCt were immobilized on Octet NTA biosensor (Sartorius) incubated in an $Octet^{Red}$ 384 system (ForteBio). The functionalized sensors were then washed for 120 s in binding buffer composed of 150 mM NaCl, 20 mM Tris-HCl, pH 8 - BSA (1 mg/mL) before dipping for 600 s into solutions of liposomes diluted in binding buffer - BSA to a final concentration of 5.0, 1.5 or 0.5 mM. Dissociation of the liposome/protein complexes was then monitored in binding buffer - BSA for 300 s. All the experiments were performed in duplicate on two different sensors to account for potential experimental artifacts due to inter-sensor variability. In all cases, potential non-specific interactions were monitored using a sensor coated with the fusion His-Streptavidin as a negative control. The curves were processed using BiaEvaluation software (Biacore).

Recombinant mammalian expression plasmids

Plasmids encoding EGFP-Rab5 was kindly provided by Philip D. Stahl (Washington University, St. Louis, MO) to our group. Plasmids pcDNA VP3 FL and pcDNA VP3 P2 (P2 all reversed) were constructed by Valli and collaborators in a previous study (Valli et al., 2012) and kindly provided by José F. Rodríguez (CSIC, Madrid, Spain) to our group. The plasmids encoding point mutant VP3

proteins ($K_{157}D$, $R_{159}D$, $H_{198}D$ and $R_{200}D$) were obtained by site-directed mutagenesis. For this purpose, the plasmid pcDNA VP3 FL was used as template DNA in polymerase chain reactions (PCR) together with oligonucleotide primer pairs containing changed nucleotides in order to generate the point mutations (*SI Appendix*, Table 1). PCRs were carried out using Pfu DNA polymerase (PB-L, Argentina) and the following conditions: initial DNA denaturation at 95°C for 5 min followed by 30 cycles of 95°C for 1 min, 65°C for 1 min and 72°C for 6 min and a final extension at 72°C for 10 min. The size of the amplified products was corroborated by agarose gel electrophoresis. In order to degrade the plasmid mold, the PCR mixtures were incubated with *Dpn*I endonuclease (ThermoFisher Scientific, USA) at 37°C for 2 h followed by heating at 80°C for 20 min. Aliquots of those reactions were transformed into competent *E. coli* DH10B cells (Invitrogen, USA). Colonies carrying the mutated plasmids were selected in LB plates containing ampicillin (100 µg/mL). Plasmids were purified using the EasyPure® Plasmid MiniPrep Kit (TransGen Biotech Co., Ltd, China) and the introduction of mutations was confirmed by nucleotide sequencing (Macrogen service, South Korea). Alignments and prediction of amino acid sequences were performed using the Aligner and Translator tools from the JustBio website ("JustBio," n.d.).

Transient transfections and indirect immunofluorescence assay

QM7 cells were grown on coverslips in an M24 multi-well plate for 12 h to approximately 70% confluence and then plasmids were transfected employing Lipofectamine 3000 (number L300015; Thermo Fisher, Argentina) following the manufacturer's recommendations. After 24 h p.i., the cells were fixed with 4% paraformaldehyde (PFA) for 15 min at room temperature (RT), washed with PBS (pH 7.4), and permeabilized with 0.05% saponin in PBS containing 0.2% BSA for 20 min at RT. Then the cells were incubated with anti-VP3 primary antibodies overnight (ON) at 4°C in a humidity chamber, and after extensive washing, cells were incubated with secondary antibodies conjugated with Alexa Fluor Cy3 for 1 h 30 min, followed by extensive washes in PBS. The coverslips were mounted in Mowiol plus Hoechst and analyzed by Confocal Laser Scanning Microscopy (CLSM). Images were captured using an Olympus FluoView TM FV1000 confocal microscope (Olympus, Argentina) with FV10-ASW (version 01.07.00.16) software and processed using the ImageJ software (Schindelin et al., 2012). For quantification of VP3 cellular distribution (**Fig. 2D**), the percentage of cells with vesicular distribution of the red signal was calculated out of approximately 30 cells per construct and experiment. For quantification of the co-localization of VP3 and either EGFP-Rab5 or EGFP-2xFYVE, the Manders M_2 coefficient was calculated out of approximately 30 cells per construct and experiment (*SI Appendix*, Fig. S3 and **Fig. 3A**, respectively). The M2 coefficient, which reflects co-localization of signals, is defined as the ratio of the total intensities of magenta image pixels for which the intensity in the blue channel is above zero to the total intensity in the magenta channel. JACoP plugin was utilized to determine M2 (Bolte and Cordelières, 2006). For VP3 puncta co-distributing with EEA1 and GST-2xFYVE the number of puncta co-distributing for the three signals was manually determined out of approximately 40 cells per construct and experiment per 200 µm² (**Fig. 3B**).

Reverse genetics

For the generation of recombinant IBDV we used a modification of the reverse genetics system described by Qi and coworkers (Qi et al., 2007), in which the full-length sequences of the IBDV segments, flanked by a hammerhead ribozyme at the 5'-end and a hepatitis delta ribozyme at the 3'-end, are expressed under the control of an RNA polymerase II promoter. For its construction, the complete segments of IBDV Soroa were amplified from viral dsRNA using a sequence independent amplification method (Potgieter et al., 2009) and cloned in plasmid pJET1.2 (Thermo Fisher Scientific). The hammerhead ribozymes, specific for each segment, are based in the HamRz-R, described by Yanay and cols. (Yanai et al., 2006), with 10 nucleotides of sequence complementary to each IBDV segment stabilizing Stem I. At the 3'-end, we used the sequence of the antigenomic hepatitis delta ribozyme HDVagrz SC (Ghanem et al., 2011). DNA fragments containing the ribozyme sequences were constructed by PCR-based gene synthesis with oligonucleotides designed by the Assembly PCR Oligo Maker software (Rydzanicz et al., 2005).

Each PCR-amplified IBDV full-length segment were cloned, flanked by the corresponding hammerhead ribozyme and HDVagrz SC, between the *Eco*RI and *Not*I sites of plasmid pCAGEN [a gift from Connie Cepko; Addgene plasmid # 11160; (Matsuda and Cepko, 2004a)] by Gibson assembly (Gibson et al., 2009). The correctness of the sequences in both plasmids, pCAGEN.Hmz.SegA.Hdz (SegA) and pCAGEN.Hmz.SegB.Hdz (SegB), was assessed by sequencing (Eurofins Scientific). The plasmid pCAGEN.Hmz.SegA.R_{200}D.Hdz (SegA.R_{200}D) was purchased to GenScript and the mutation was verified by sequencing of the complete plasmid (Eurofins Scientific).

Recombinant viruses foci forming units assay

QM7 cells were grown in M24 multi-well plates for 12 h to approximately 90-95% confluency and then 800 ng (400 ng of plasmid with each segment) were transfected by using Lipofectamine 2000 (number 11668027; Thermo Fisher, Spain) following the manufacturer's recommendations. When performing single segment transfections (SegA, SegB and SegA.R_{200}D), 400 ng of the plasmid pCAGIG (a gift from Connie Cepko; Addgene plasmid #11159; (Matsuda and Cepko, 2004b) was added to 400 ng of those containing the viral segments to reach a total of 800 ng of total DNA per transfection. pCAGIG is a mammalian expression vector that shares the backbone with the pCAGEN vector used for the expression of the viral segments. The following transfections were performed in triplicate: SegA, SegB, SegA.R_{200}D, SegA+SegB or SegA.R_{200}D+ SegB. At 8 h post-transfection (p.t.) the supernatants were discarded and the monolayers were recovered for further plating on M6 multi-well plates containing non transfected QM7 cells. For monolayers transfected with SegA, SegB, SegA.R_{200}D and SegA.R_{200}D+ SegB half of the transfected monolayer was plated on fresh cells. For SegA+SegB, which leads to the production of wild type virus, several dilutions were tested, always in triplicate. To limit virus diffusion and facilitating the foci forming Avicel RC-591 (FMC Biopolymer) was added to the M6 multi-well plates. 72 h p.i., the monolayers were 16% formaldehyde-fixated and stained with Coomassie R250 (BioRad).

Statistical analysis

One-way ANOVA followed by a Tukey's HSD (honestly significant difference) test were performed using AnalystSoft Inc., StatPlus:mac - Version v8 ("AnalystSoft Inc., StatPlus:mac - v8," n.d.). Plotting was done using the *ggplot2* package (Wickham, 2016) in R, with assistance from the RStudio software (RStudio Team, 2020).

Bioinformatics analysis

Multiple sequence alignment and the percent identity matrix were performed with Clustal OMEGA (v1.2.4) (Sievers et al., 2011) implemented at EMBL's European Bioinformatics Institute ("EMBL's European Bioinformatics Institute," n.d.). Accession numbers of the sequences: Infectious bursal disease virus (AF_140705.1); Blotched snakehead virus (YP_052872.1); Victorian trout aquabirnavirus (YP_009255397.1); Tellina virus 2 (YP_010084301.1); Yellowtail ascites virus (NP_690805.1); Infectious pancreatic necrosis virus (NP_047196.1); Tasmanian aquabirnavirus (YP_009177608.1); Lates calcarifer birnavirus (YP_010086267.1) and Tellina virus 1 (YP_009509080.1). Alignment visualization was done with the R *ggmsa* package (Zhou et al., 2022) with the assistance from the RStudio software (RStudio Team, 2020). Amino acids are colored according to their side-chain chemistry. Protein sequence logos annotation is displayed on top of the amino acid alignment.

The model of VP3 FL from IBDV ([strain Soroa, GenBank AF140705.1, residues 756-1012 (257 residues) from the polyprotein] was generated using a local copy of AlphaFold-2 (Jumper et al., 2021), installed using the open-source code available at *https://github.com/deepmind/alphafold* (accessed on 1 September 2021). Runs were performed on a Centos 7 workstation with 64 CPUs and 4 GeForce RTX 2080 Ti GPUs, using the casp14 preset and including all PDB templates present in the database. The program produces a per-residue confidence metric termed pLDTT on a scale

from 0 to 100. pLDTT values higher than 70 reflect reliable models with correct backbone predictions, and those with values higher than 90 correspond to models with both reliable backbone and side-chain orientation predictions. pLDTT values lower than 50 are a strong predictor of disorder, and regions with such values are either unstructured under physiological conditions or only structured as part of a complex.

Reagents and antibodies

Western blot and confocal laser scanning microscopy (CLSM) analyses were carried out using rabbit anti-VP3 specific sera followed by horseradish peroxidase (HRP)-conjugated anti-rabbit secondary antibodies (number A0545), purchased from Sigma-Aldrich (Buenos Aires, Argentina). For early endosomes detection by CLSM, we used anti-EEA1 mouse monoclonal antibody (1:200 dilution; BD Transduction Laboratories, 610456), and for anti-GST detection, we used Alexa Fluor 649-labelled goat anti-GST (Rockland-Inc, 600-143-200). Fluorescently labelled secondary antibodies, all diluted 1:200 from Invitrogen, included Alexa Fluor 546 donkey anti-mouse (A10036), and Alexa Fluor 546 donkey anti-rabbit (A10040).

Far-UV circular dichroism (CD) of VP3 proteins

His-VP3 FL and His-VP3 FL $R_{200}D$ at a concentration of 2 mg/ml in 50 mM Tris-HCl pH 8, 500 mM NaCl were analysed by far-UV CD (180-260 nm). CD spectra were obtained with an AVIV CD spectropolarimeter model 215 using a 0.02 cm path length cell at RT. Five successive scans were averaged and the background spectrum of the sample buffer, acquired under identical conditions, was subtracted. The resulting corrected CD intensities were then converted to Δε per residue. Secondary structure contents were estimated from the far-UV CD spectra using the CDSSTR routine (Johnson, 1999) of the DICHROWEB server (Whitmore and Wallace, 2008, 2004) run on the SP175 reference dataset (Lees et al., 2006), containing 72 proteins representing a large panel of secondary structures. Similar results were obtained on different datasets (Sreerama and Woody, 2000) or by using the CONTIN/LL routine (Provencher and Glöckner, 1981).

Coarse Grain (CG) models of VP3 constructs

Three main protein constructs derived from VP3 were considered: 1. VP3 Ct. A peptide comprising the last 36 residues of VP3 (223 to 257). VP3 Ct has an overall electrical charge of +5, and is absent from the available crystal structure of VP3. Consequently, it was assumed to be a disordered domain and was modeled as unstructured. 2. VP3 ΔNt. A shorter version of VP3 that lacks the first 81 residues leading to the Nt. It consists of the crystallized structure of the protein core (residues 82 to 222, available from the Protein Data Bank PDB ID 2R18), concatenated with the VP3 Ct peptide. As the first 9 residues of the protein core are also missing from resolved structure, they were modeled as unstructured, similar to the VP3 Ct fragment. VP3 ΔNt was selected primarily because it contains the structural information of the crystallized protein, which provides valuable insights into the protein's overall structure and function. In addition, the construct includes the Ct peptide (VP3 Ct), which is crucial for membrane binding. Although the Nt 81 residues are absent in this construct, their exclusion was found to be inconsequential in terms of evaluating the protein's binding energy and positioning on the membrane surface (compare, for example, VP3 ΔNt and VP3 FL in **Figure 5**). 3. VP3 FL. The full-length VP3 protein, which was obtained as an AlphaFold2 prediction (Jumper et al., 2021). The structure of the protein predicted by AlphaFold2 not only provided insight into the overall architecture of VP3, but it also reinforced our model of unstructured VP3 Ct. It is worth noting that the Nt 81 residues, which are absent in VP3 ΔNt, are predicted to be in a modular conformation, constituting a globular domain separated by a loop from the globular domain of the core region (crystallized residues 82 to 222). The structural information provided by the full-length VP3 model is therefore useful in understanding the interaction with lipid membranes. In addition to VP3 Ct, VP3 ΔNt, and VP3 FL, two mutants of VP3 ΔNt were simulated: VP3 ΔNt $R_{200}D$, in which R_{200} was replaced by aspartate (D), and VP3 ΔNt P2 Mut, where the whole P2 region (R_{200}, H_{198}, R_{159}, and K_{157}) was replaced by D. All proteins

were modeled with the MARTINI force-field (De Jong et al., 2013) [whenever needed, the secondary structure of the non-disordered protein domains was restrained by means of the ElNeDyn elastic network model (elnedyn22)] (Periole et al., 2009; Poma et al., 2017). In this case, harmonic potentials with a force constant of 1000 kJ mol^{-1} nm^2 were applied between backbone particles separated by less than 1.4 nm. In the construction of VP3 ΔNt, elastic network restrictions were applied to residues 91 to 220, which was the fragment resolved from by crystallography. However, in VP3 FL, the elastic network was applied to all globular domains, while leaving the linkers and the last 36 residues at the Ct unrestricted.

Molecular Theory calculations

The Molecular Theory (MT) used to assess protein adsorption is detailed in references (Chiarpotti et al., 2021; Ramírez et al., 2019). Briefly, this mean-field method yields the distribution of macromolecules in an anisotropic system, through the minimization of a model free-energy functional that accounts for electrostatic and steric interactions, the configurational and translational entropy of the macromolecules, the translational entropy of the free species (protons, hydroxyls, and salt ions) and the acid-base equilibrium of all ionizable molecules in the system. In the present case, the membrane was modeled as a dielectric slab of thickness h, with a dielectric constant ε_M, which is in contact with a solution of dielectric constant ε_S. Far from the membrane ($z \to \infty$), the solution is in contact with an infinite bulk that contains the proteins (1 μM concentration), all the free species, and a fixed pH=8. The rigid membrane contained 15% of ionizable groups on its surface, in order to mimic the 5% of ternary ionizable PI3P. One third of these groups were assigned a pK_a of 2.5, corresponding to the phosphate group of the glycerol moiety, while the pK_a for the rest was set to 6.5, corresponding to the phosphoesther groups of inositol. MT requires the input of a large set of protein conformations, which are subsequently reweighted by the theory. These conformations were generated by Molecular Dynamics simulations of the proteins in water. VP3 Ct, VP3 ΔNt, VP3 FL, VP3 ΔNt $R_{200}D$, and VP3 ΔNt P2 Mut, were modeled using MARTINI-2.2 parameters (Marrink et al., 2007). The proteins were hydrated in MARTINI polarizable water. As stated before, the proteins globular segments (residues 92-222 in VP3 FL, VP3 ΔNt and its mutants, and residues 7-79 additionally in VP3 FL) were restricted through the application of the elastic network ElNeDyn (Marrink et al., 2007) with a spring constant of 1000 kJ.mol^{-1} applied to backbone beads (BB) within a cutoff distance of 1.4 nm. Each protein was simulated for 100 ns, after equilibration, in the NPT ensemble using GROMACS 2021.3. A cluster analysis was performed in order to obtain the most representative conformations of the simulated ensemble. This method groups conformations by structural similarity, using the root mean squared deviation (RMSD) of the coordinates calculated for all conformer pairs along the trajectory, clustering structures with RMSD ≤ 0.3 nm. This procedure leads to 50 conformers for each protein construct. Each conformer was subsequently rotated 30 times randomly to produce a set of 1500 configurations for the MT calculations.

Molecular Dynamics Simulations of VP3 on a lipid bilayer

MARTINI-2.2 was also used to model the lipid molecules in our MD simulations. The bilayer was assembled using insane utility (Wassenaar et al., 2015), while hydration with polarizable water molecules and ions was performed with the solvate utility of the GROMACS package. The bilayer had a symmetric lipid composition of 30% 1,2-dioleoyl-sn-glycero-3-phosphocholine (DOPC), 65% of 1,2-dioleoyl-sn-glycero-3-phosphoethanolamine (DOPE) and 5% 1,2-dioleoyl-sn-glycero-3-phosphatidylinositol-3-phosphate (PI3P), leading to a lipid composition of 111:231:18 (DOPC, DOPE, and PI3P) in each leaflet. The protein was placed at a distance of 10 nm from the membrane surface, to avoid a possible initial binding bias. The system was then equilibrated and finally simulated for 500 ns. Both equilibration and production were in the NPT ensemble. A semi-isotropic Parinello-Rahman barostat (Parrinello and Rahman, 1981) with a 12 ps time constant, and lateral and normal compressibilities of 3×10^{-4} bar^{-1} were used to keep the pressure at 1.0 bar.

The v-rescale thermostat, with a time constant of 1 ps, was used to keep the temperature at 325 K. In all cases the integration timestep was 20 fs. Long range electrostatics were calculated using the particle mesh Ewald (PME) method (Darden et al., 1993) with a real-space cut-off of 1.2 nm.

Acknowledgements

This project was partially supported by: the National Agency for Scientific and Technological Promotion, Ministry of Science, Technology and Innovation, through grants PICT 2016-0528 and 2019-01324 to L.R.D; PICT 2015-2210 to F.A.Z; PICT 2019-01889 to L.M.P. and PICT 2020-3795 to M.G.D.P; the National Scientific and Technical Research Council through grants PIP 2015-2017 11220150100114CO and 2021-2023 11220200103139CO to L.R.D.; 2021-2023 11220200103195CO to L.M.P. and 11220200103223CO to M.G.D.P.; and by the National University of Cuyo through grants 2013-2015 M006, 2016-2018 M029, 2019-2021 M071 and 2022-2024 M012 to L.R.D. For stays performed by L.R.D. in the laboratory of Structural Virology at the Institut Pasteur in Paris, we are grateful for the support of National University of Cuyo through the Teaching Staff Mobility Program in 2018-2019, the Ministry of Education through the Program scholarships for training abroad in Science and Technology (BEC.AR 2018), and the International Union of Biochemistry and Molecular Biology (IUBMB) through a “2020 Mid-Career Research Fellowship”. The work in Madrid was supported by grants from the Spanish Ministry of Science and Innovation (PID2020-113287RB-I00) and the Comunidad Autónoma de Madrid (P2018/NMT-4389) to JRC. At the IHEM, we sincerely appreciate Elisa Bocanegra, Norberto Domizio, and Jorge Ibañez for valuable technical assistance in CLSM handling. At the Institut Pasteur in Paris, we are grateful to Gérard Pehau-Arnaudet and the staff at the Ultrastructural BioImaging core facility for image acquisition and analysis; to Patrick England and Sébastien Brûlé and the staff of the Molecular Biophysics platform for purified protein analyses, CD and BLI assays, to Stéphane Petres and members at the Production and Purification of Recombinant Proteins Technological Platform, and to the staff of the Proteomics platform.

Additional information

Author Contributions

I.F., E.B., F.A.R., M.G.D.P. and L.R.D. designed research; F.A.Z., P.G.C., A.F.I., S.D., E.M., V.A., M.O.A., M.E.C., L.M.P., L.S., V.V.G., M.V.C., C.A., J.M.R., and L.R.D. performed research; I.F., E.B., M.O.A., D.L., M.G.D.P., F.A.R., and L.R.D. analyzed data; J.R.C., O.T., M.I.C. and F.A.R. contributed new reagents/analytic tools; and L.R.D. and M.G.D.P. wrote the paper.

Additional files

Supplemental Figures

References

AnalystSoft Inc. n.d) **StatPlus:mac**

Baltimore D 1971) **Expression of animal virus genomes** *Bacteriol Rev* **35** https://doi.org/10.1128/BR.35.3.235-241.1971

Banani SF, Lee HO, Hyman AA, Rosen MK 2017) **Biomolecular condensates: organizers of cellular biochemistry** *Nat Rev Mol Cell Biol* **18**:285–298 https://doi.org/10.1038/NRM.2017.7

Bolte S, Cordelières FP 2006) **A guided tour into subcellular colocalization analysis in light microscopy** *J Microsc* **224**:213–232 https://doi.org/10.1111/j.1365-2818.2006.01706.x

Brodrick AJ, Broadbent AJ 2023) **The Formation and Function of Birnaviridae Virus Factories** *Int J Mol Sci* **24** https://doi.org/10.3390/IJMS24108471

Burd CG, Emr SD 1998) **Phosphatidylinositol(3)-phosphate signaling mediated by specific binding to RING FYVE domains** *Mol Cell* **2**:157–62

Casañas A, Navarro A, Ferrer-Orta C, González D, Rodríguez JF, Verdaguer N 2008) **Structural Insights into the Multifunctional Protein VP3 of Birnaviruses** *Structure* **16**:29–37 https://doi.org/10.1016/j.str.2007.10.023

Chiarpotti M V., Longo GS, Del Pópolo MG 2021) **Nanoparticles modified with cell penetrating peptides: Assessing adsorption on membranes containing acidic lipids** *Colloids Surf B Biointerfaces* **197** https://doi.org/10.1016/J.COLSURFB.2020.111373

Coulibaly F, Chevalier C, Gutsche I, Pous J, Navaza J, Bressanelli S, Delmas B, Rey FA 2005) **The birnavirus crystal structure reveals structural relationships among icosahedral viruses** *Cell* **120**:761–772 https://doi.org/10.1016/j.cell.2005.01.009

Darden T, York D, Pedersen L 1993) **Particle mesh Ewald: An N·log(N) method for Ewald sums in large systems** *J Chem Phys* **98**:10089–10092 https://doi.org/10.1063/1.464397

De Jong DH, Singh G, Bennett WFD, Arnarez C, Wassenaar TA, Schäfer L V., Periole X, Tieleman DP, Marrink SJ. 2013) **Improved parameters for the martini coarse-grained protein force field** *J Chem Theory Comput* **9**:687–697 https://doi.org/10.1021/ct300646g

Delgui LR, Rodriguez JF, Colombo MI 2013) **The Endosomal Pathway and the Golgi Complex Are Involved in the Infectious Bursal Disease Virus Life Cycle** *J Virol* **87**:8993–9007 https://doi.org/10.1128/JVI.03152-12

Delmas B, Attoui H, Ghosh S, Malik YS, Mundt E, Vakharia VN 2019) **ICTV virus taxonomy profile: Birnaviridae** *Journal of General Virology* **100**:5–6 https://doi.org/10.1099/jgv.0.001185

no date) **EMBL's European Bioinformatics Institute. n.d. https://www.ebi.ac.uk/ no date** https://www.ebi.ac.uk/

Olson F, Hunt FCS C A, Vail DP W J 1979) **Preparation of liposomes of defined size distribution by extrusion through polycarbonate membranes** *Biochim Biophys Acta* **557**:9–

23 https://doi.org/10.1016/0005-2736(79)90085-3

Fernandes F, Chen K, Ehrlich LS, Jin J, Chen MH, Medina GN, Symons M, Montelaro R, Donaldson J, Tjandra N, Carter CA 2011) **Phosphoinositides Direct Equine Infectious Anemia Virus Gag Trafficking and Release** *Traffic* https://doi.org/10.1111/j.1600-0854.2010.01153.x

Gaullier J-M, Simonsen A, D'Arrigo A, Bremnes B, Stenmark H, Aasland R 1998) **FYVE fingers bind PtdIns(3)P** *Nature* **394**:432–433 https://doi.org/10.1038/28767

Ghanem A, Kern A, Conzelmann K-K 2011) **Significantly improved rescue of rabies virus from cDNA plasmids** *Eur J Cell Biol* **91**:10–16 https://doi.org/10.1016/j.ejcb.2011.01.008

Gibson DG, Young L, Chuang R-Y, Venter JC, Hutchison CA, Smith HO 2009) **Enzymatic assembly of DNA molecules up to several hundred kilobases** *Nat Methods* **6** https://doi.org/10.1038/nmeth.1318

Gillooly DJ, Morrow IC, Lindsay M, Gould R, Bryant NJ, Gaullier JM, Parton RG, Stenmark H 2000) **Localization of phosphatidylinositol 3-phosphate in yeast and mammalian cells** *EMBO Journal* **19**:4577–4588 https://doi.org/10.1093/emboj/19.17.4577

Gimenez MC, Issa M, Sheth J, Colombo MI, Terebiznik MR, Delgui LR 2020) **Phosphatidylinositol 3-Phosphate Mediates the Establishment of Infectious Bursal Disease Virus Replication Complexes in Association with Early Endosomes** *J Virol* **95**:e02313–20 https://doi.org/10.1128/jvi.02313-20

Gimenez MC, Zanetti FA, Terebiznik MR, Colombo MI, Delgui LR 2018) **Infectious Bursal Disease Virus Hijacks Endosomal Membranes as the Scaffolding Structure for Viral Replication** *J Virol* **92**:e01964–17 https://doi.org/10.1128/JVI.01964-17

Gorbalenya AE, Pringle FM, Zeddam JL, Luke BT, Cameron CE, Kalmakoff J, Hanzlik TN, Gordon KHJ, Ward VK 2002) **The palm subdomain-based active site is internally permuted in viral RNA-dependent RNA polymerases of an ancient lineage** *J Mol Biol* **324**:47–62 https://doi.org/10.1016/S0022-2836(02)01033-1

Gorvel JP, Chavrier P, Zerial M, Gruenberg J 1991) **rab5 controls early endosome fusion in vitro** *Cell* **64**:915–25

Johnson WC 1999) **Analyzing Protein Circular Dichroism Spectra for Accurate Secondary Structures** *Proteins* **35**:307–312 https://doi.org/10.1002/(SICI)1097-0134(19990515)35:3

Jumper J, Evans R, Pritzel A, Green T, Figurnov M, Ronneberger O, Tunyasuvunakool K, Bates R, Žídek A, Potapenko A, Bridgland A, Meyer C, Kohl SAA, Ballard AJ, Cowie A, Romera-Paredes B, Nikolov S, Jain R, Adler J, Back T, Petersen S, Reiman D, Clancy E, Zielinski M, Steinegger M, Pacholska M, Berghammer T, Bodenstein S, Silver D, Vinyals O, Senior AW, Kavukcuoglu K, Kohli P, Hassabis D 2021) **Highly accurate protein structure prediction with AlphaFold** *Nature* **596**:583–589 https://doi.org/10.1038/s41586-021-03819-2

n.d) **JustBio.**

Kairys V, Baranauskiene L, Kazlauskiene M, Matulis D, Kazlauskas E 2019) **Binding affinity in drug design: experimental and computational techniques** *Expert Opinion on Drug Discovery* **14** https://doi.org/10.1080/17460441.2019.1623202

Kolli S, Meng X, Wu X, Shengjuler D, Cameron CE, Xiang Y, Deng J 2015) **Structure-Function Analysis of Vaccinia Virus H7 Protein Reveals a Novel Phosphoinositide Binding Fold Essential for Poxvirus Replication** *J Virol* **89**:2209–2219 https://doi.org/10.1128/JVI.03073-14/ASSET/F1575F5D-784E-4FD0-9DDB-A2B374935CCA/ASSETS/GRAPHIC/ZJV9990900510007.JPEG

Komada M, Kitamura N 1995) **Growth factor-induced tyrosine phosphorylation of Hrs, a novel 115-kilodalton protein with a structurally conserved putative zinc finger domain** *Mol Cell Biol* **15**:6213–6221 https://doi.org/10.1128/MCB.15.11.6213

Koonin E V., Dolja V V., Krupovic M, Varsani A, Wolf YI, Yutin N, Zerbini FM, Kuhn JH 2020) **Global Organization and Proposed Megataxonomy of the Virus World** *Microbiology and Molecular Biology Reviews* **84** https://doi.org/10.1128/MMBR.00061-19/SUPPL_FILE/MMBR.00061-19-S0001.PDF

Lees JG, Miles AJ, Wien F, Wallace BA 2006) **A reference database for circular dichroism spectroscopy covering fold and secondary structure space** *Bioinformatics* **22**:1955–1962 https://doi.org/10.1093/BIOINFORMATICS/BTL327

Lombardo E, Maraver A, Castón JR, Rivera J, Fernández-Arias A, Serrano A, Carrascosa JL, Rodriguez JF 1999) **VP1, the putative RNA-dependent RNA polymerase of infectious bursal disease virus, forms complexes with the capsid protein VP3, leading to efficient encapsidation into virus-like particles** *J Virol* **73**:6973–83

Luque D, Rivas G, Alfonso C, Carrascosa JL, Rodríguez JF, Castón JR 2009a) **Infectious bursal disease virus is an icosahedral polyploid dsRNA virus** *Proc Natl Acad Sci U S A* **106**:2148–52 https://doi.org/10.1073/pnas.0808498106

Luque D, Saugar I, Rejas MT, Carrascosa JL, Rodríguez JF, Castón JR 2009b) **Infectious Bursal Disease Virus: Ribonucleoprotein Complexes of a Double-Stranded RNA Virus** *J Mol Biol* **386**:891–901 https://doi.org/10.1016/j.jmb.2008.11.029

Maraver A, Oña A, Abaitua F, González D, Clemente R, Ruiz-Díaz JA, Castón JR, Pazos F, Rodriguez JF 2003) **The oligomerization domain of VP3, the scaffolding protein of infectious bursal disease virus, plays a critical role in capsid assembly** *J Virol* **77**:6438–49

Marrink SJ, Risselada HJ, Yefimov S, Tieleman DP, De Vries AH 2007) **The MARTINI force field: Coarse grained model for biomolecular simulations** *Journal of Physical Chemistry B* **111**:7812–7824 https://doi.org/10.1021/jp071097f

Matsuda T, Cepko CL 2004a) **Electroporation and RNA interference in the rodent retina in vivo and in vitro** *Proc Natl Acad Sci U S A* **101**:16–22 https://doi.org/10.1073/pnas.2235688100

Matsuda T, Cepko CL 2004b) **Electroporation and RNA interference in the rodent retina in vivo and in vitro** *Proc Natl Acad Sci U S A* **101**:16–22 https://doi.org/10.1073/PNAS.2235688100

Mcnulty S, Bornmann W, Schriewer J, Werner C, Smith SK, Olson VA, Damon IK, Buller RM, Heuser J, Kalman D 2010) **Multiple Phosphatidylinositol 3-Kinases Regulate Vaccinia Virus Morphogenesis** *PLoS One* **5** https://doi.org/10.1371/JOURNAL.PONE.0010884

Miles AJ, Wallace BA 2018) **CDtoolX, a downloadable software package for processing and analyses of circular dichroism spectroscopic data** *Protein Science* **27**:1717–1722 https://doi.org/10.1002/pro.3474

Nascimbeni AC, Codogno P, Morel E 2017) **Local detection of PtdIns3P at autophagosome biogenesis membrane platforms** *Autophagy* **13**:1602–1612 https://doi.org/10.1080/15548627.2017.1341465

Parrinello M, Rahman A 1981) **Polymorphic transitions in single crystals: A new molecular dynamics method** *J Appl Phys* **52**:7182–7190 https://doi.org/10.1063/1.328693

Periole X, Cavalli M, Marrink SJ, Ceruso MA 2009) **Combining an elastic network with a coarse-grained molecular force field: Structure, dynamics, and intermolecular recognition** *J Chem Theory Comput* **5**:2531–2543 https://doi.org/10.1021/CT9002114/SUPPL_FILE/CT9002114_SI_001.PDF

Poma AB, Cieplak M, Theodorakis PE 2017) **Combining the MARTINI and Structure-Based Coarse-Grained Approaches for the Molecular Dynamics Studies of Conformational Transitions in Proteins** *J Chem Theory Comput* **13**:1366–1374 https://doi.org/10.1021/ACS.JCTC.6B00986/ASSET/IMAGES/LARGE/CT-2016-00986K_0005.JPEG

Potgieter AC, Page NA, Liebenberg J, Wright IM, Landt O, van Dijk AA 2009) **Improved strategies for sequence-independent amplification and sequencing of viral double-stranded RNA genomes** *J Gen Virol* **90**:1423–1432 https://doi.org/10.1099/vir.0.009381-0

Provencher SW, Glöckner J 1981) **Estimation of Globular Protein Secondary Structure from Circular Dichroism** *Biochemistry* **20**:33–37 https://doi.org/10.1021/bi00504a006

Puffer BA, Watkins SC, Montelaro RC 1998) **Equine infectious anemia virus Gag polyprotein late domain specifically recruits cellular AP-2 adapter protein complexes during virion assembly** *J Virol* **72**:10218–10221 https://doi.org/10.1128/JVI.72.12.10218-10221.1998

Qi X, Gao Y, Gao H, Deng X, Bu Z, Xiaoyan Wang, Fu C, Xiaomei Wang 2007) **An improved method for infectious bursal disease virus rescue using RNA polymerase II system** *J Virol Methods* **142**:81–88 https://doi.org/10.1016/j.jviromet.2007.01.021

Ramírez PG, Del Pópolo MG, Vila JA, Szleifer I, Longo GS 2019) **Adsorption and insertion of polyarginine peptides into membrane pores: The trade-off between electrostatics, acid-base chemistry and pore formation energy** *J Colloid Interface Sci* **552**:701–711 https://doi.org/10.1016/J.JCIS.2019.05.087

Reddy V, Lymar E, Hu M, Hainfeld JF 2005) **5 nm Gold-Ni-NTA Binds His Tags** *Microscopy and Microanalysis* **11**:1118–1119 https://doi.org/10.1017/S1431927605507712

Reddy VRAP, Campbell EA, Wells J, Simpson J, Nazki S, Hawes PC, Broadbent AJ 2022) **Birnaviridae Virus Factories Show Features of Liquid-Liquid Phase Separation and Are Distinct from Paracrystalline Arrays of Virions Observed by Electron Microscopy** *J Virol* **96** https://doi.org/10.1128/jvi.02024-21

RStudio Team 2020) **RStudio: Integrated Development Environment for R**

Rydzanicz R, Zhao XS, Johnson PE 2005) **Assembly PCR oligo maker: a tool for designing oligodeoxynucleotides for constructing long DNA molecules for RNA production** *Nucleic Acids Res* **33**:W521–5 https://doi.org/10.1093/nar/gki380

Saugar I, Irigoyen N, Luque D, Carrascosa JL, Rodríguez JF, Castón JR 2010) **Electrostatic interactions between capsid and scaffolding proteins mediate the structural**

polymorphism of a double-stranded RNA virus *J Biol Chem* **285**:3643–50 https://doi.org/10.1074/jbc.M109.075994

Schindelin J, Arganda-Carreras I, Frise E, Kaynig V, Longair M, Pietzsch T, Preibisch S, Rueden C, Saalfeld S, Schmid B, Tinevez J-Y, White DJ, Hartenstein V, Eliceiri K, Tomancak P, Cardona A 2012) **Fiji: an open-source platform for biological-image analysis** *Nat Methods* **9**:676–682 https://doi.org/10.1038/nmeth.2019

Shah NB, Duncan T M 2014) **Bio-layer interferometry for measuring kinetics of protein-protein interactions and allosteric ligand effects** *J Vis Exp* https://doi.org/10.3791/51383

Sievers F, Wilm A, Dineen D, Gibson TJ, Karplus K, Li W, Lopez R, McWilliam H, Remmert M, Söding J, Thompson JD, Higgins DG 2011) **Fast, scalable generation of high-quality protein multiple sequence alignments using Clustal Omega** *Mol Syst Biol* **7** https://doi.org/10.1038/MSB.2011.75

Simonsen A, Lippe R, Christoforidis S, Gaullier J-M, Brech A, Callaghan J, Toh B-H, Murphy C, Zerial M, Stenmark H 1998) **EEA1 links PI(3)K function to Rab5 regulation of endosome fusion** *Nature* **1998**:494–498 https://doi.org/10.1038/28879

Sreerama N, Woody RW 2000) **Estimation of protein secondary structure from circular dichroism spectra: Comparison of CONTIN, SELCON, and CDSSTR methods with an expanded reference set** *Anal Biochem* **287**:252–260 https://doi.org/10.1006/abio.2000.4880

Stenmark H, Aasland R, Toh BH, D'Arrigo A 1996) **Endosomal localization of the autoantigen EEA1 is mediated by a zinc-binding FYVE finger** *J Biol Chem* **271**:24048–54

Tanzi GO, Piefer AJ, Bates P 2003) **Equine infectious anemia virus utilizes host vesicular protein sorting machinery during particle release** *J Virol* **77**:8440–8447 https://doi.org/10.1128/JVI.77.15.8440-8447.2003

Valli A, Busnadiego I, Maliogka V, Ferrero D, Castón JR, Rodríguez JF, García JA 2012) **The VP3 Factor from Viruses of Birnaviridae Family Suppresses RNA Silencing by Binding Both Long and Small RNA Duplexes** *PLoS One* **7** https://doi.org/10.1371/journal.pone.0045957

Walker PJ, Siddell SG, Lefkowitz EJ, Mushegian AR, Adriaenssens EM, Alfenas-Zerbini P, Davison AJ, Dempsey DM, Dutilh BE, García ML, Harrach B, Harrison RL, Hendrickson RC, Junglen S, Knowles NJ, Krupovic M, Kuhn JH, Lambert AJ, Łobocka M, Nibert ML, Oksanen HM, Orton RJ, Robertson DL, Rubino L, Sabanadzovic S, Simmonds P, Smith DB, Suzuki N, Van Dooerslaer K, Vandamme AM, Varsani A, Zerbini FM 2021) **Changes to virus taxonomy and to the International Code of Virus Classification and Nomenclature ratified by the International Committee on Taxonomy of Viruses** *Arch Virol* **166**:2633–2648 https://doi.org/10.1007/S00705-021-05156-1

Wassenaar TA, Ingólfsson HI, Böckmann RA, Tieleman DP, Marrink SJ 2015) **Computational lipidomics with insane: A versatile tool for generating custom membranes for molecular simulations** *J Chem Theory Comput* **11**:2144–2155 https://doi.org/10.1021/acs.jctc.5b00209

Whitmore L, Wallace BA 2008) **Protein secondary structure analyses from circular dichroism spectroscopy: Methods and reference databases** *Biopolymers* **89**:392–400 https://doi.org/10.1002/bip.20853

Whitmore L, Wallace BA 2004) **DICHROWEB, an online server for protein secondary structure analyses from circular dichroism spectroscopic data** *Nucleic Acids Res* **32** https://

doi.org/10.1093/nar/gkh371

Wickham H 2016) **ggplot2: Elegant Graphics for Data Analysis** Springer-Verlag New York

Wills JW, Craven RC 1991) **Form, function, and use of retroviral gag proteins** *Aids* **5**:639–654 https://doi.org/10.1097/00002030-199106000-00002

Yanai H, Hayashi Y, Watanabe Y, Ohtaki N, Kobayashi T, Nozaki Y, Ikuta K, Tomonaga K 2006) **Development of a novel Borna disease virus reverse genetics system using RNA polymerase II promoter and SV40 nuclear import signal** *Microbes Infect* **8**:1522–1529 https://doi.org/10.1016/j.micinf.2006.01.010

Zhou L, Feng T, Xu S, Gao F, Lam TT, Wang Q, Wu T, Huang H, Zhan L, Li L, Guan Y, Dai Z, Yu G 2022) **. ggmsa: a visual exploration tool for multiple sequence alignment and associated data** *Brief Bioinform* **23** https://doi.org/10.1093/BIB/BBAC222

Author information

Flavia A Zanetti[#]
Instituto de Ciencia y Tecnología “Dr. Cesar Milstein”, Consejo Nacional de Investigaciones Científicas y Técnicas (CONICET), Buenos Aires, Argentina
ORCID iD: 0000-0002-4337-4163

[#]contributed equally to this work.

Ignacio Fernández[#]
Institut Pasteur, Université Paris Cité, Structural Virology Unit, Paris, France
ORCID iD: 0000-0003-2632-8111

[#]contributed equally to this work.

Eduard Baquero
Institut Pasteur, Université Paris Cité, Structural Virology Unit, Paris, France
ORCID iD: 0000-0002-4701-4181

Pablo Guardado-Calvo
Institut Pasteur, Université Paris Cité, Structural Virology Unit, Paris, France
ORCID iD: 0000-0001-7292-5270

Andres Ferrino-Iriarte
Institut Pasteur, Université Paris Cité, Structural Virology Unit, Paris, France
ORCID iD: 0000-0003-0821-556X

Sarah Dubois
Université Paris Cité, INSERM UMR-S1151, CNRS UMR-S8253, Institut Necker Enfants Malades, Paris, France
ORCID iD: 0009-0000-7504-7135

Etienne Morel
Université Paris Cité, INSERM UMR-S1151, CNRS UMR-S8253, Institut Necker Enfants Malades, Paris, France
ORCID iD: 0000-0002-4763-4954

Victoria Alfonso
Instituto de Agrobiotecnología y Biología Molecular (IABIMO), Instituto Nacional de Tecnología Agropecuaria (INTA), Consejo Nacional de Investigaciones Científicas y Técnicas (CONICET), Buenos Aires, Argentina
ORCID iD: 0000-0002-9167-6107

Milton O Aguilera
Instituto de Histología y Embriología de Mendoza, Universidad Nacional de Cuyo (UNCuyo), Consejo Nacional de Investigaciones Científicas y Técnicas (CONICET), Centro Universitario M5502JMA, Mendoza, Argentina
ORCID iD: 0000-0002-5413-769X

María E Celayes
Instituto de Histología y Embriología de Mendoza, Universidad Nacional de Cuyo (UNCuyo), Consejo Nacional de Investigaciones Científicas y Técnicas (CONICET), Centro Universitario M5502JMA, Mendoza, Argentina
ORCID iD: 0009-0005-6905-6218

Luis M Polo
Instituto de Histología y Embriología de Mendoza, Universidad Nacional de Cuyo (UNCuyo), Consejo Nacional de Investigaciones Científicas y Técnicas (CONICET), Centro Universitario M5502JMA, Mendoza, Argentina
ORCID iD: 0000-0001-9257-6127

Laila Suhaiman[†]
Instituto Interdisciplinario de Ciencias Básicas (ICB), Consejo Nacional de Investigaciones Científicas y Técnicas (CONICET), Mendoza, Argentina
ORCID iD: 0000-0001-8376-2673

[†]Present address: Instituto de Medicina y Biología Experimental de Cuyo (IMBECU) - Consejo Nacional de Investigaciones Científicas y Técnicas (CONICET), Facultad de Ciencias Médicas, Universidad Nacional de Cuyo (UNCuyo), Mendoza, Argentina.

Vanesa V Galassi
Instituto Interdisciplinario de Ciencias Básicas (ICB), Consejo Nacional de Investigaciones Científicas y Técnicas (CONICET), Mendoza, Argentina, Facultad de Ciencias Exactas y Naturales, Universidad Nacional de Cuyo (UNCuyo), Mendoza, Argentina
ORCID iD: 0000-0002-8058-6069

María V Chiarpotti[††]
Instituto Interdisciplinario de Ciencias Básicas (ICB), Consejo Nacional de Investigaciones Científicas y Técnicas (CONICET), Mendoza, Argentina, Facultad de Ciencias Exactas y Naturales, Universidad Nacional de Cuyo (UNCuyo), Mendoza, Argentina
ORCID iD: 0000-0003-2480-0494

††Present address: AI Proteins, Boston, USA.

Carolina Allende
Department of Structure of Macromolecules, Centro Nacional de Biotecnología (CNB-CSIC), Madrid, Spain
ORCID iD: 0000-0002-0967-9481

Javier M Rodríguez
Department of Structure of Macromolecules, Centro Nacional de Biotecnología (CNB-CSIC), Madrid, Spain
ORCID iD: 0000-0003-0146-9903

José R Castón
Department of Structure of Macromolecules, Centro Nacional de Biotecnología (CNB-CSIC), Madrid, Spain
ORCID iD: 0000-0003-2350-9048

Diego Lijavetzky
Instituto de Biología Agrícola de Mendoza, Universidad Nacional de Cuyo (UNCuyo), Consejo Nacional de Investigaciones Científicas y Técnicas (CONICET), Mendoza, Argentina
ORCID iD: 0000-0003-4207-3067

Oscar Taboga
Instituto de Agrobiotecnología y Biología Molecular (IABIMO), Instituto Nacional de Tecnología Agropecuaria (INTA), Consejo Nacional de Investigaciones Científicas y Técnicas (CONICET), Buenos Aires, Argentina
ORCID iD: 0000-0001-9575-3045

María I Colombo
Instituto de Histología y Embriología de Mendoza, Universidad Nacional de Cuyo (UNCuyo), Consejo Nacional de Investigaciones Científicas y Técnicas (CONICET), Centro Universitario M5502JMA, Mendoza, Argentina
ORCID iD: 0000-0002-2676-3845

Mario G Del Pópolo
Instituto Interdisciplinario de Ciencias Básicas (ICB), Consejo Nacional de Investigaciones Científicas y Técnicas (CONICET), Mendoza, Argentina, Facultad de Ciencias Exactas y Naturales, Universidad Nacional de Cuyo (UNCuyo), Mendoza, Argentina
ORCID iD: 0000-0002-1435-2424

Félix A Rey
Institut Pasteur, Université Paris Cité, Structural Virology Unit, Paris, France
ORCID iD: 0000-0002-9953-7988

Laura R Delgui
Instituto de Histología y Embriología de Mendoza, Universidad Nacional de Cuyo (UNCuyo), Consejo Nacional de Investigaciones Científicas y Técnicas (CONICET), Centro Universitario M5502JMA, Mendoza, Argentina, Facultad de Ciencias Exactas y Naturales, Universidad Nacional de Cuyo (UNCuyo), Mendoza, Argentina
ORCID iD: 0000-0002-3647-3593

ldelgui@mendoza-conicet.gob.ar; ldelgui@fcm.uncu.edu.ar

Editors

Reviewing Editor
Mauricio Comas-Garcia
Universidad Autónoma de San Luis Potosí, San Luis Potos, Mexico

Senior Editor
Wendy Garrett
Harvard T.H. Chan School of Public Health, Boston, United States of America

Reviewer #1 (Public review):

Summary:

Zanetti et al use biophysical and cellular assays to investigate the interaction of the birnavirus VP3 protein with the early endosome lipid PI3P. The major novel finding is that association of the VP3 protein with an anionic lipid (PI3P) appears to be important for viral replication, as evidenced through a cellular assay on FFUs.

Strengths:

Support previously published claims that VP3 associates with early endosome membrane, potentially through binding to PI3P. The finding that mutating a single residue (R200) critically affects early endosome binding and that the same mutation also inhibits viral replication suggests a very important role for this binding in the viral life cycle.

Weaknesses:

The manuscript is relatively narrowly focused: the specifics of the bi-molecular interaction between the VP3 of an unusual avian virus and a host cell lipid (PIP3). Further, the affinity of this interaction is low and its specificity relative to other PIPs is not tested, leading to questions about whether VP3-PI3P binding is relevant.

https://doi.org/10.7554/eLife.97261.2.sa2

Reviewer #3 (Public review):

Summary:

infectious bursal disease virus (IBDV) is a birnavirus and an important avian pathogen. Interestingly, IBDV appears to be a unique dsRNA virus that uses early endosomes for RNA replication that is more common for +ssRNA viruses such as for example SARS-CoV-2.

This work builds on previous studies showing that IBDV VP3 interacts with PIP3 during virus replication. The authors provide further biophysical evidence for the interaction and map the interacting domain on VP3.

Strengths:

Detailed characterization of the interaction between VP3 and PIP3 identified R200D mutation as critical for the interaction. Cryo-EM data show that VP3 leads to membrane deformation.

Comments on revisions:

I have no further comments. The authors have addressed my questions and concerns. I congratulate the authors on their work!

https://doi.org/10.7554/eLife.97261.2.sa1

Author response:

The following is the authors' response to the current reviews.

> ***Public Reviews:***
>
> ***Reviewer #1 (Public review):***
>
> *Summary:*
>
> *Zanetti et al use biophysical and cellular assays to investigate the interaction of the birnavirus VP3 protein with the early endosome lipid PI3P. The major novel finding is that association of the VP3 protein with an anionic lipid (PI3P) appears to be important for viral replication, as evidenced through a cellular assay on FFUs.*
>
> *Strengths:*
>
> *Support previously published claims that VP3 associates with early endosome membrane, potentially through binding to PI3P. The finding that mutating a single residue (R200) critically affects early endosome binding and that the same mutation also inhibits viral replication suggests a very important role for this binding in the viral life cycle.*
>
> *Weaknesses:*
>
> *The manuscript is relatively narrowly focused: the specifics of the bi-molecular interaction between the VP3 of an unusual avian virus and a host cell lipid (PIP3). Further, the affinity of this interaction is low and its specificity relative to other PIPs is not tested, leading to questions about whether VP3-PI3P binding is relevant.*

Regarding the manuscript's focus, we challenge the notion that studying a single bi-molecular interaction makes the scope of the paper overly narrow. This interaction—between VP3 and PI3P—plays a critical role in the replication of the birnavirus, which is the central theme of our work. Moreover, identifying and understanding such distinct interactions is a fundamental aspect of molecular virology, as they shed light on the precise mechanisms that viruses exploit to hijack the host cell machinery. Consequently, far from being narrowly focused, we believe our work contributes to the broader understanding of host-pathogen interactions.

As for the low affinity of the VP3-PI3P interaction, we argue that this is not a limitation but rather a biologically relevant feature. As discussed in the manuscript, the moderate strength of this interaction is likely critical for regulating the turnover rate of VP3/endosomal PI3P complexes, which in turn could optimize viral replication efficiency. A stronger affinity might trap VP3 on the endosomal membrane, whereas weaker interactions might reduce its ability to efficiently target PI3P. Thus, the observed affinity may reflect a fine-tuned balance that supports the viral life cycle.

With regard to specificity, we emphasize that in the context of the paper, we refer to biological specificity, which is not necessarily the same as chemical specificity. The binding of PI3P to early endosomes is "biologically" preconditioned by the distribution of PI3P within the cell. PI3P is predominantly localized in endosomal membranes, which "biologically

precludes" interference from other PIPs due to their distinct cellular distributions. Moreover, while early endosomes also contain other anionic lipids, our work demonstrates that among these, PI3P plays a distinctive role in VP3 binding. This highlights its functional relevance in the context of early endosome dynamics.

> ***Reviewer #3 (Public review):***
>
> *Summary:*
>
> *Infectious bursal disease virus (IBDV) is a birnavirus and an important avian pathogen. Interestingly, IBDV appears to be a unique dsRNA virus that uses early endosomes for RNA replication that is more common for +ssRNA viruses such as for example SARS-CoV-2. This work builds on previous studies showing that IBDV VP3 interacts with PIP3 during virus replication. The authors provide further biophysical evidence for the interaction and map the interacting domain on VP3.*
>
> *Strengths:*
>
> *Detailed characterization of the interaction between VP3 and PIP3 identified R200D mutation as critical for the interaction. Cryo-EM data show that VP3 leads to membrane deformation.*

We thank the reviewer for the feedback.

The following is the authors' response to the original reviews.

> ***Public Reviews:***
>
> ***Reviewer #1 (Public Review):***
>
> *Summary:*
>
> *Zanetti* et al*. use biophysical and cellular assays to investigate the interaction of the birnavirus VP3 protein with the early endosome lipid PI3P. The major novel finding is that the association of the VP3 protein with an anionic lipid (PI3P) appears to be important for viral replication, as evidenced through a cellular assay on FFUs.*
>
> *Strengths:*
>
> *Supports previously published claims that VP3 may associate with early endosomes and bind to PI3P-containing membranes. The claim that mutating a single residue (R_{200}) critically affects early endosome binding and that the same mutation also inhibits viral replication suggests a very important role for this binding in the viral life cycle.*
>
> *Weaknesses:*
>
> *The manuscript is relatively narrowly focused: one bimolecular interaction between a host cell lipid and one protein of an unusual avian virus (VP3-PI3P). Aspects of this interaction have been described previously. Additional data would strengthen claims about the specificity and some technical issues should be addressed. Many of the core claims would benefit from additional experimental support to improve consistency.*

Indeed, our group has previously described aspects of the VP3-PI3P interaction, as indicated in lines 100-105 from the manuscript. In this manuscript, however, we present biochemical and biophysical details that have not been reported before about how VP3 connects with early endosomes, showing that it interacts directly with the PI3P. Additionally, we have now identified a critical residue in VP3—the R_{200}—for binding to PI3P and its key role in the viral

life cycle. Furthermore, the molecular dynamics simulations helped us come up with a mechanism for VP3 to connect with PI3P in early endosomes. This constitutes a big step forward in our understanding of how these "*non-canonical*" viruses replicate.

We have now incorporated new experimental and simulation data; and have carefully revised the manuscript in accordance with the reviewers' recommendations. We are confident that these improvements have further strengthened the manuscript.

> ***Reviewer #2 (Public Review):***
>
> *Summary:*
>
> *Birnavirus replication factories form alongside early endosomes (EEs) in the host cell cytoplasm. Previous work from the Delgui lab has shown that the VP3 protein of the birnavirus strain infectious bursal disease virus (IBDV) interacts with phosphatidylinositol-3-phosphate (PI3P) within the EE membrane (Gimenez et al., 2018, 2020). Here, Zanetti* et al*. extend this previous work by biochemically mapping the specific determinants within IBDV VP3 that are required for PI3P binding* in vitro*, and they employ* in silico *simulations to propose a biophysical model for VP3-PI3P interactions.*
>
> *Strengths:*
>
> *The manuscript is generally well-written, and much of the data is rigorous and solid. The results provide deep knowledge into how birnaviruses might nucleate factories in association with EEs. The combination of approaches (biochemical, imaging, and computational) employed to investigate VP3-PI3P interactions is deemed a strength.*
>
> *Weaknesses:*
>
> *(1) Concerns about the sources, sizes, and amounts of recombinant proteins used for co-flotation: Figures 1A, 1B, 1G, and 4A show the results of co-flotation experiments in which recombinant proteins (control His-FYVE v. either full length or mutant His VP3) were either found to be associated with membranes (top) or non-associated (bottom). However, in some experiments, the total amounts of protein in the top + bottom fractions do not appear to be consistent in control v. experimental conditions. For instance, the Figure 4A western blot of His-2xFYVE following co-flotation with PI3P+ membranes shows almost no detectable protein in either top or bottom fractions.*

Liposome-based methods, such as the co-flotation assay, are well-established and widely regarded as the preferred approach for studying protein-phosphoinositide interactions. However, this approach is rather qualitative, as density gradient separation reveals whether the protein is located in the top fractions (bound to liposomes) or the bottom fractions (unbound). Our quantifications aim to demonstrate differences in the bound fraction between liposome populations with and without PI3P. Given the setting of the co-flotation assays, each protein-liposome system [2xFYVE-PI3P(-), 2xFYVE-PI3P(+), VP3-PI3P(-), or VP3-PI3P(+)] is assessed separately, and even if the experimental conditions are homogeneous, it is not surprising to observe differences in the protein level between different experiments. Indeed, the revised version of the manuscript includes membranes with more similar band intensities, as depicted in the new versions of Figures 1 and 4.

> *Reading the paper, it was difficult to understand which source of protein was used for each experiment (i.e.,* E. coli *or baculovirus-expressed), and this information is contradicted in several places (see lines 358-359 v. 383-384). Also, both the control protein and the His-VP3-FL proteins show up as several bands in the western blots, but they don't appear to be consistent with the sizes of the proteins stated on lines 383-384.*

> *For example, line 383 states that His-VP3-FL is ~43 kDa, but the blots show triplet bands that are all below the 35 kDa marker (Figures 1B and 1G). Mass spectrometry information is shown in the supplemental data (describing the different bands for His-VP3-FL) but this is not mentioned in the actual manuscript, causing confusion. Finally, the results appear to differ throughout the paper (see Figures 1B v. 1G and 1A v. 4A).*

Thank you for pointing out these potentially confusing points in the previous version of the manuscript. Indeed, we were able to produce recombinant VP3 from the two sources: Baculovirus and *Escherichia coli*. Initially, we opted for the baculovirus system, based on evidence from previous studies showing that it was suitable for ectopic expression of VP3. Subsequently, we successfully produced VP3 using *Escherichia coli*. On the other side, the fusion proteins His-2xFYVE and GST-2xFYVE were only produced in the prokaryotic system, also following previous reported evidence. We confirmed that VP3, produced in either system, exhibited similar behavior in our co-flotation and bio-layer interferometry (BLI) assays. However, the results of co-flotation and BLI assays shown in Figs. 1 and 4 were performed using the His-VP3 FL, His-VP3 FL R_{200}D and His-VP3 FL DCt fusion proteins produced from the corresponding baculoviruses. We have clarified this in the revised version of our manuscript. Please, see lines 430-432.

Additionally, we have made clear that the His-VP3 FL protein purification yielded four distinct bands, and we confirmed their VP3 identity through mass spectrometry in the revised version of the manuscript. Please, see lines 123-124.

Finally, we replaced membranes for Figs. 4A and 1G (left panel) with those with more similar band intensities. Please, see the new version of Figures 1 and 4.

> *(2) Possible "other" effects of the R_{200}D mutation on the VP3 protein. The authors performed mutagenesis to identify which residues within patch 2 on VP3 are important for association with PI3P. They found that a VP3 mutant with an engineered R_{200}D change (i) did not associate with PI3P membranes in co-floatation assays, and (ii) did not co-localize with EE markers in transfected cells. Moreover, this mutation resulted in the loss of IBDV viability in reverse genetics studies. The authors interpret these results to indicate that this residue is important for "mediating VP3-PI3P interaction" (line 211) and that this interaction is essential for viral replication. However, it seems possible that this mutation abrogated other aspects of VP3 function (e.g., dimerization or other protein/RNA interactions) aside from or in addition to PI3P binding. Such possibilities are not mentioned by the authors.*

The arginine amino acid at position 200 of VP3 is not located in any of the protein regions associated with its other known functions: VP3 has a dimerization domain located in the second helical domain, where different amino acids across the three helices form a total of 81 interprotomeric close contacts; however, R_{200} is not involved in these contacts (Structure. 2008 Jan;16(1):29-37, doi:10.1016/j.str.2007.10.023); VP3 has an oligomerization domain mapped within the 42 C-terminal residues of the polypeptide, i.e., the segment of the protein composed by the residues at positions 216-257 (*J Virol*. 2003 Jun;77(11):6438–6449, doi: 10.1128/jvi.77.11.6438-6449.2003); VP3's ability to bind RNA is facilitated by a region of positively-charged amino acids, identified as P1, which includes K_{99}, R_{102}, K_{105}, and K_{106} (*PLoS One*. 2012;7(9):e45957, doi: 10.1371/journal.pone.0045957). Furthermore, our findings indicate that the R_{200}D mutant retains a folding pattern similar to the wild-type protein, as shown in Figure 4B. All these lead us to conclude that the loss of replication capacity of R_{200}D viruses results from impaired, or even loss of, VP3-PI3P interaction.

We agree with the reviewer that this is an important point and have accordingly addressed it in the Discussion section of the revised manuscript. Please, see lines 333-346.

(3) Interpretations from computational simulations. The authors performed computational simulations on the VP3 structure to infer how the protein might interact with membranes. Such computational approaches are powerful hypothesis-generating tools. However, additional biochemical evidence beyond what is presented would be required to support the authors' claims that they "unveiled a two-stage modular mechanism" for VP3-PI3P interactions (see lines 55-59). Moreover, given the biochemical data presented for R_{200}D VP3, it was surprising that the authors did not perform computational simulations on this mutant. The inclusion of such an experiment would help tie together the in vitro and in silico data and strengthen the manuscript.

We acknowledge that the wording used in the previous version of the manuscript may have overstated the "unveiling" of the two-stage binding mechanism of VP3. Our intention was to propose a potential mechanism, that is consistent both with the biophysical experiments and the molecular simulations. In the revised version of the manuscript, we have tempered these claims and framed them more appropriately.

Regarding the simulations for the R_{200}D VP3 mutant, these simulations were indeed performed and included in the original manuscript as part of Figure S14 in the Supplementary Information. However, we realize that this was not sufficiently emphasized in the main text, an oversight on our part. We have now revised the manuscript to highlight these results more clearly.

Additionally, to further strengthen the connection between experimental and simulation trends, we have now included a new figure in the Supplementary Information (Figure S15). This figure depicts the binding energy of VP3 ΔNt and two of its mutants, VP3 ΔNt R_{200}D and VP3 ΔNt P2 Mut, as a function of salt concentration. The results show that as the number of positively charged residues in VP3 is systematically reduced, the binding of the protein to the membrane becomes weaker. The effect is more pronounced at lower salt concentrations, which highlights the weight of electrostatic forces on the adsorption of VP3 on negatively charged membranes. Please, see Supplementary Information (Figure S15).

Reviewer #3 (Public Review):

Summary:

Infectious bursal disease virus (IBDV) is a birnavirus and an important avian pathogen. Interestingly, IBDV appears to be a unique dsRNA virus that uses early endosomes for RNA replication that is more common for +ssRNA viruses such as for example SARS-CoV-2.

This work builds on previous studies showing that IBDV VP3 interacts with PIP3 during virus replication. The authors provide further biophysical evidence for the interaction and map the interacting domain on VP3.

Strengths:

Detailed characterization of the interaction between VP3 and PIP3 identified R_{200}D mutation as critical for the interaction. Cryo-EM data show that VP3 leads to membrane deformation.

Weaknesses:

The work does not directly show that the identified R_{200} residues are directly involved in VP3-early endosome recruitment during infection. The majority of work is done with transfected VP3 protein (or in vitro*) and not in virus-infected cells. Additional controls*

> *such as the use of PIP3 antagonizing drugs in infected cells together with a colocalization study of VP3 with early endosomes would strengthen the study.*
>
> *In addition, it would be advisable to include a control for cryo-EM using liposomes that do not contain PIP3 but are incubated with HIS-VP3-FL. This would allow ruling out any unspecific binding that might not be detected on WB.*
>
> *The authors also do not propose how their findings could be translated into drug development that could be applied to protect poultry during an outbreak. The title of the manuscript is broad and would improve with rewording so that it captures what the authors achieved.*

In previous works from our group, we demonstrated the crucial role of the VP3 P2 region in targeting the early endosomal membranes and for viral replication, including the use of PI3K inhibitors to deplete PI3P, showing that both the control RFP-2xFYVE and VP3 lost their ability to associate with the early endosomal membranes and reduces the production of an infective viral progeny (*J Virol*. 2018 May 14;92(11):e01964-17, doi: 10.1128/jvi.01964-17; *J Virol*. 2021 Feb 24;95(6):e02313-20, doi: 10.1128/jvi.02313-20). In the present work, to further characterize the role of R_{200} in binding to early endosomes and for viral replication, we show that: i) the transfected VP3 R_{200}D protein loses the ability to bind to early endosomes in immunofluorescence assays (Figure 2E and Figure 3); ii) the recombinant His-VP3 FL R_{200}D protein loses the ability to bind to liposomes PI3P(+) in co-flotation assays (Figure 4A); and, iii) the mutant virus R_{200}D loses replication capacity (Figure 4C).

Regarding the cryo-electron microscopy observation, we verified that there is no binding of gold particles to liposomes PI3P(-) when they are incubated solely with the gold-particle reagent, or when they are pre-incubated with the gold-particle reagent with either His-2xFYVE or His-VP3 FL. We have incorporated a new panel in Figure 1C showing a representative image of these results. Please, see lines 143-144 in the revised version of our manuscript and our revised version of Figure 1C.

We have replaced the title of the manuscript by a more specific one. Thus, our current is " On the Role of VP3-PI3P Interaction in Birnavirus Endosomal Membrane Targeting".

Regarding the question of how our findings could be translated into drug development, indeed, VP3-PI3P binding constitutes a good potential target for drugs that counteract infectious bursal disease. However, we did not mention this idea in the manuscript, first because it is somewhat speculative and second because infected farms do not implement any specific treatment. The control is based on vaccination.

> ***Recommendations for the authors:***
>
> ***Reviewer #1 (Recommendations For The Authors):***
>
> *Critical issues to address:*
>
> *(1) The citations in the important paragraph on lines 101-5 are not identifiable. These references are described as showing that VP3 is associated with EEs via P2 and PI3P, which is basically what this paper also shows. The significant advance here is unclear.*

We apologize for this mistake. These citations are identifiable in the revised version of the manuscript (lines 100-105). As mentioned before, in this manuscript we present biochemical and biophysical details that have not been reported before about how VP3 connects with early endosomes, showing that it interacts directly with the PI3P. Additionally, we have now identified a critical residue in VP3 P2—the R_{200}—for binding to PI3P and its key role in the viral life cycle. Furthermore, the molecular dynamics simulations helped us come up with a

mechanism for VP3 to connect with PI3P in early endosomes. This constitutes a big step forward in our understanding of how these "*non-canonical*" viruses replicate.

> *(2) Even if all the claims were to be clearly supported through major revamping, authors should make the significance of knowing that this protein binds to early endosomes through PI3P more clear?*

Thank you for the recommendation, which aligns with a similar suggestion from Reviewer #2. In response, we have revised the significance paragraph to emphasize the mechanistic aspects of our findings. Please refer to lines 62–67 in the revised manuscript.

> *(3) Flotation assay shows binding, but this is not quantitative. An estimate of a Kd would be useful. BLI experiments suggest that half of the binding disappears at 0.5 mM, implying a very low binding affinity.*

We agree with the reviewer that our biophysical and molecular simulation results suggest a specific but weak interaction of VP3 with PI3P bearing membranes. Indeed, our previous version of the manuscript already contained a paragraph in this regard. Please, see lines 323-332 in the revised version of the manuscript.

From a biological point of view, a low binding affinity of VP3 for the endosomes may constitute an advantage for the virus, in the sense that its traffic through the endosomes may be short lived during its infectious cycle. Indeed, VP3 has been demonstrated to be a "multifunctional" protein involved in several processes of the viral cycle (detailed in lines 84-90), and in our laboratory we have shown that the Golgi complex and the endoplasmic reticulum are organelles where further viral maturation occurs. Taking all of this into account, a high binding affinity of VP3 for endosomes could result in the protein becoming trapped on the endosomal membrane, potentially hindering the progression of the viral infection within the host cell.

> *(4) There are some major internal inconsistencies in the data: Figure 1B quantifies VP3-FL T/B ratio ~4 (which appears inconsistent with the image shown, as the T lanes are much lighter than the B) whereas apparently the same experiment in Figure 1G shows it to be ~0.6. With the error bars shown, these results would appear dramatically different from each other, despite supposedly measuring the same thing. The same issue with the FYVE domain between Figures 1A and 4A.*

We appreciate the reviewer's comment, as it made us aware of an error in Figure 1B. There, the mean value for the VP3-FL Ts/B ratio is 3.0786 for liposomes PI3P(+) and 0.4553 for liposomes PI3P(-) (Please, see the new bar graph on Figure 1B). This may have occurred because, due to the significance of these experiments, we performed multiple rounds of quantification in search of the most suitable procedure for our observations, leading to a mix-up of data sets. Anyway, it's possible that these corrected values still seem inconsistent given that T lanes are much lighter than the B for VP3-FL in the image shown. Flotation assays are quite labor-intensive and, at least in our experience, yield fairly variable results in terms of quantification. To illustrate this point, the following image shows the three experiments conducted for Figure 1B, where it is clear that, despite producing visually distinct images, all three yielded the same qualitative observation. For Figure 1B, we chose to present the results from experiment #2. However, all three experiments contributed to a Ts/B ratio of 3.0786 for His-VP3 FL, which may account for the apparent inconsistency when focusing solely on the image in Figure 1B.

Author response image 1.

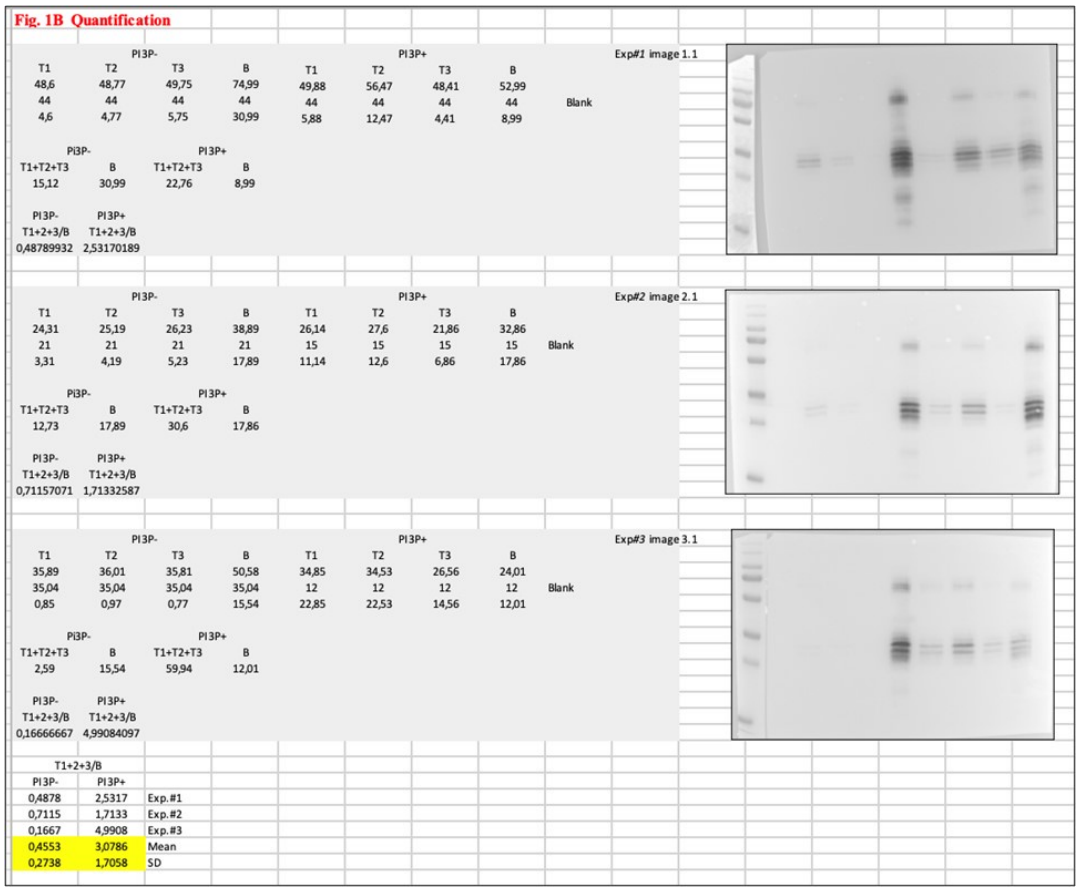

We acknowledge that, at first glance, some inconsistencies may appear in the results, and we have thoroughly discussed the best approach for quantification. However, we believe the observations are robust in terms of reproducibility and reliable, as the VP3-PI3P interaction was consistently validated by comparison with liposomes lacking PI3P, where no binding was observed.

> *(5) Comparison of PA (or PI) to PI3P at the same molar concentration is inappropriate because PI3P has at least double charge. The more interesting question about specificity would be whether PI45P2 (or even better PI35P2) binds or not. Without this comparison, no claim to specificity can be made.*

For us, "specificity" refers to the requirement of a phosphoinositide in the endosomal membrane for VP3 binding. Phosphoinositides have a conspicuous distribution among cellular compartments, and knowing that VP3 associates with early endosomes, our specificity assays aimed to demonstrate that PI3P is strictly required for the binding of VP3. To validate this, we used PI (lacking the phosphate group) and PA (lacking the inositol group) despite their similar charges. In spite of the potential chemical interactions between VP3 and various phosphoinositides, our experimental results suggest that the virus specifically targets endosomal membranes by binding to PI3P, a phosphoinositide present only in early endosomes.

That said, we agree with the reviewer's point and consider adequate to smooth our specificity claim in the manuscript as follows: "We observed that His-VP3 FL bound to liposomes PI3P(+),

but not to liposomes PA or PI, reinforcing the notion that a phosphoinositide is required since neither a single negative charge nor an inositol ring are sufficient to promote VP3 binding to liposomes (SI Appendix, Fig. S2)" (Lines 136-139).

> *(6) In the EM images, many of the gold beads are inside the vesicles. How do they cross the membranes?*

They do not cross the membrane. Our EM images are two-dimensional projections, meaning that the gold particles located on top or beneath the plane appear to be inside the liposome.

> *(7) Images in Figure 2D are very low quality and do not show the claimed difference between any of the mutants. All red signal looks basically cytosolic in all images. It is not clear what criteria were used for the quantification in Figure 2E. The same issue is in Figure 2E, where no red WT puncta are observable at all. Consistently, there is minimal colocalization in the quantification in Figure S3, which appears to show no significant differences between any of the mutants, in direct contradiction to the claim in the manuscript.*

We apologize for the poor quality of panels in Figures 2D and 2E. Unfortunately, this was due to the PDF conversion of the original files. Please, check the high-quality version of Figure 2. As suggested by reviewers #2 and #3, we have incorporated zoomed panels, which help the reader to better see the differences in distribution.

As mentioned in the legend to Figure 2, the quantification in Figure 2D was performed by calculating the percentage of cells with punctuated fluorescent red signal (showing VP3 distribution) for each protein. The data were then normalized to the P2 WT protein, which is the VP3 wild type.

Figure S3 certainly shows a tendency which positively correlates with the results shown in Figure 3, where we used FYVE to detect PI3P on endosomes and observed significantly less co-localization when VP3 bears its P2 region all reversed or lacks the R_{200}

> *(8) The only significant differences in colocalization are in Figure 3B, whose images look rather dramatically different from the rest of the manuscript, leading to some concern about repeatability. Also, it is unclear how colocalization is quantified, but this number typically cannot be above 1. Finally, it is unclear what is being colocalized here: with three fluorescent components, there are 3 possible binary colocalizations and an additional ternary colocalization.*

We thank the reviewer for pointing out those aspects related to Figure 3. The experiments performed for Figure 3B were conducted by a collaborator abroad handling the purified GST-2xFYVE, which recognizes endogenous PI3P, while the rest of the cell biology experiments were conducted in our laboratory in Argentina. This is why they are aesthetically different. We have made an effort in homogenizing the way they look for the revised version of the manuscript. Please, see the new version of Figure 3.

For quantification of the co-localization of VP3 and EGFP-2xFYVE (Figure 3A), the Manders M2 coefficient was calculated out of approximately 30 cells per construct and experiment. The M2 coefficient, which reflects co-localization of signals, is defined as the ratio of the total intensities of magenta image pixels for which the intensity in the blue channel is above zero to the total intensity in the magenta channel. JACoP plugin was utilized to determine M2. For VP3 puncta co-distributing with EEA1 and GST-FYVE (Figure 3B), the number of puncta co-distributing for the three signals was manually determined out of approximately 40 cells per construct and experiment per 200 μm². We understand that Manders or Pearson coefficients, typically ranging between 0 and 1, is the most commonly used method to quantify co-

localizing immunofluorescent signals; however, this “manual” method has been used and validated in previous published manuscripts [Figures 3 and 7 from (Morel et al., 2013); Figure 7 in (Khaldoun et al., 2014); and Figure 4 in (Boukhalfa et al., 2021)].

> *(9) SegA/B plasmids are not introduced, and it is not clear what these are or how this assay is meant to work. Where are the foci forming units in the images of Figure 4C? How does this inform on replication? Again, this assay is not quantitative, which is essential here: does the R_{200} mutant completely kill activity (whatever that is here)? Or reduce it somewhat?*

We apologize for the missing information. Segments A and B are basically the components of the IBDV reverse genetics system. For their construction, we used a modification of the system described by Qi and coworkers (Qi et al., 2007), in which the full length sequences of the IBDV RNA segments A and B, flanked by a hammerhead ribozyme at the 5’-end and the hepatitis delta ribozyme at the 3’-end, were expressed under the control of an RNA polymerase II promoter within the plasmids pCAGEN.Hmz.SegA.Hdz (SegA) and pCAGEN.Hmz.SegB.Hdz (SegB). For this specific experiment we generated a third plasmid, pCAGEN.Hmz.SegA.R_{200}D.Hdz (SegA.R_{200}D), harboring a mutant version of segment A cDNA containing the R_{200}D substitution. Then, QM7 cells were transfected with the plasmids SegA, SegB or Seg.R_{200}D alone (as controls) or with a mixture of plasmids SegA+SegB (wild type situation) or SegA.R_{200}D+SegB (mutant situation). At 8 h post transfection (p.t.), when the new viruses have been able to assemble starting from the two segments of RNA, the cells were recovered and re-plated onto fresh non-transfected cells for revealing the presence (or not) of infective viruses. At 72 h post-plating, the generation of foci forming units (FFUs) was revealed by Coomassie staining. As expected, single-transfections of SegA, SegB or Seg.R_{200}D did not produce FFUs and, as shown in Figure 4C, the transfection of SegA+SegB produced detectable FFUs (the three circles in the upper panel) while no FFUs (the three circles in the lower panel) were detected after the transfection of SegA.R_{200}D+SegB (Figure 4C). This system is quantitative, since the FFUs detected 72 h post-plating are quantifiable by simply counting the FFUs. However, since no FFUs were detected after the transfection of SegA.R_{200}D+SegB, evidenced by a complete monolayer of cells stained blue, we did not find any sense in quantifying. In turn, this drastic observation indicates that viruses bearing the VP3 R_{200}D mutation lose their replication ability (is “dead”), demonstrating its crucial role in the infectious cycle.

We agree with the reviewer that a better explanation was needed in the manuscript, so we have incorporated a paragraph in the results section of our revised version of the manuscript (lines 209-219).

> *(10) Why pH 8 for simulation?*

The Molecular Theory calculations were performed at pH 8 for consistency with the experimental conditions used in our biophysical assays. These biophysical experiments were also performed at pH 8, following the conditions established in the original study where VP3 was first purified for crystallization (DOI: 10.1016/j.str.2007.10.023).

> *(11) There is minimal evidence for the sequential binding model described in the abstract. The simulations do not resolve this model, nor is truly specific PI3P binding shown.*

In response to your concerns, we would like to emphasize that our simulations provide robust evidence supporting the two more important aspects of the sequential binding model: 1) Membrane Approach: In all simulations, VP3 consistently approaches the membrane via its positively charged C-terminal (Ct) region. 2) PI3P Recruitment: Once the protein is positioned

flat on the membrane surface, PI3P is unequivocally recruited to the positively charged P2 region. The enrichment of PI3P in the proximity to the protein is clearly observed and has been quantified via radial distribution functions, as detailed in the manuscript and supplementary material.

While we understand that opinions may vary on the sufficiency of the data to fully validate the model, we believe the results offer meaningful insights into the proposed binding mechanism. That said, we acknowledge that the specificity of VP3 binding may not be restricted solely to PI3P but could extend to phosphoinositides in general. To address this, we performed the new set of co-flotation experiments which are discussed in detail in our response to point 5.

> ***Reviewer #2 (Recommendations For The Authors):***
>
> *(1) Line 1: Consider changing the title to better reflect the mostly biochemical and computational data presented in the paper: "Mechanism of Birnavirus VP3 Interactions with PI3P-Containing Membranes". There are no data to show hijacking by a virus presented.*

We appreciate this recommendation, which was also expressed by reviewer #3. Additionally, we thank for the suggested title. We have replaced the title of the manuscript by a more specific one. Thus, our current is

"On the Role of VP3-PI3P Interaction in Birnavirus Endosomal Membrane Targeting".

> *(2) Lines 53-54 and throughout: Consider rephrasing "demonstrate" to "validate" to give credit to Gimenez et al., 2018, 2022 for discovery.*

Thanks for the suggestion. We have followed it accordingly. Please see line 52 from our revised version of the manuscript.

> *(3) Line 56-59 and throughout: Consider tempering and rephrasing these conclusions that are based mostly on computational data. For example, change "unveil" to "suggest" or another term.*

We have now modified the wording throughout the manuscript.

> *(4) The abstract could also emphasize that this study sought to map the resides within VP3 that are important for P13P interaction.*

Thanks for the suggestion. We have followed it accordingly. Please, see lines 53-55 from our revised version of the manuscript.

> *(5) Lines 63-69: This Significance paragraph seems tangential. The findings in this paper aren't at all related to the evolutionary link between birnaviruses and positive-strand RNA viruses. The significance of the work for me lies in the deep biochemical/biophysical insights into how a viral protein interacts with membranes to nucleate its replication factory.*

We have re-written the significance paragraph highlighting the mechanistic aspect of our findings. Please, see lines 62-67 in our revised version of the manuscript.

> *(6) Line 74: Please define "IDBV" abbreviation.*

We apologize for the missing information. We have defined the IBDV abbreviation in our revised version of the manuscript (please, see line 73).

> *(7) Line 88: Please define "pVP2" abbreviation.*

We apologize for the missing information. We have defined the pVP2 abbreviation in our revised version of the manuscript (please, see line 87).

> *(8) Lines 101-105: Please change references (8, 9, 10) to be consistent with the rest of the manuscript (names, year).*

We apologize for this mistake. These citations are identifiable and consistent in the revised version of the manuscript (lines 100-105).

> *(9) Line 125: For a broad audience, consider explaining that recombinant His-2xFYVE domain is known to exhibit PI3P-binding specificity and was used as a positive control.*

Thanks for the recommendation. We have incorporated a brief explanation supporting the use of His-2xFYVE as a positive control in our revised version of the manuscript. Please, see lines 127-129.

> *(10) Lines 167-171: The quantitative data in Figure S3 shows that there was a non-significant co-localization coefficient of the R_{200}D mutant. For transparency, this should be stated in the Results section when referenced.*

We agree with this recommendation. We have clearly mentioned it in the revised version of the manuscript. Please, see lines 177-179. Also, we have referred this fact when introducing the assays performed using the purified GST-2xFYVE, shown in Figure 3. Please, see lines 182-184.

> *(11) Lines 156 and 173: These Results section titles have nearly identical wording. Consider rephrasing to make it distinct.*

We agree with the reviewer's observation. In fact, we sought to do it on purpose as for them to be a "wordplay", but we understand that could result in a awkwarded redundancy. So, in the revised version of the manuscript, both titles are:

Role of VP3 P2 in the association of VP3 with the EE membrane (line 163).

VP3 P2 mediates VP3-PI3P association to EE membranes (line 182).

> *(12) Line 194: Is it alternatively possible that the R_{200}D mutant lost its capacity to dimerize, and that in turn impacted PI3P interaction?*

Thanks for the relevant question. VP3 was crystallized and its structure reported in (Casañas et al., 2008) (DOI: 10.1016/j.str.2007.10.023). In that report, the authors showed that the two VP3 subunits associate in a symmetrical manner by using the crystallographic two-fold axes. Each subunit contributes with its 30% of the total surface to form the dimer, with 81 interprotomeric close contacts, including polar bonds and van der Waals contacts. The authors identified the group of residues involved in these interactions, among which the R_{200} is not included. Addittionally, the authors determined that the interface of the VP3 dimer in crystals is biologically meaningful (not due to the crystal packing).

To confirm that the lack of binding was not due to misfolding of the mutant, we compared the circular dichroism spectra of mutant and wild type proteins, without detecting significant differences (shown in Figure 4B). These observations do not exclude the possibility mentioned by the reviewer, but constitute solid evidences, we believe, to validate our observations.

> *(13) Lines 231-243: Consider changing verbs to past tense (i.e., change "is" to "was") for the purposes of consistency and tempering.*

Thanks for the recommendation, we have proceeded as suggested. Please, see lines 249-262 in our revised version of the manuscript.

> *(14) Lines 306-308: Is there any information about whether it is free VP3 (v. VP3 complexed in RNP) that binds to membrane? I am just trying to wrap my head around how these factories form during infection.*

Thanks for pointing this out. We first observed that in infected cell, all the components of the RNPs [VP3, VP1 (the viral polymerase) and the dsRNA] were associated to the endosomes. Since by this moment it had been already elucidated that VP3 "wrapped" de dsRNA within the RNPs (Luque et al., 2009) (DOI: 10.1016/j.jmb.2008.11.029), we sought that VP3 was most probably leading this association. We answered yes after studying its distribution, also endosome-associated, when ectopically expressed. These results were published in (Delgui et al., 2013) (DOI: 10.1128/jvi.03152-12).

Thus, in our subsequent studies, we have worked with both, the infection-derived or the ectopically expressed VP3, to advance in elucidating the mechanism by which VP3 hijacks the endosomal membranes and its relevancy for viral replication, reported in this current manuscript.

> *(15) Lines 320-334: This last paragraph discussing evolutionary links between birnaviruses and positive-strand RNA viruses seems tangential and distracting. Consider reducing or removing.*

Thanks for highlighting this aspect of our work. Maybe difficult to follow, but in the context of other evidences reported for the *Birnaviridae* family of viruses, we strongly believe that there is an evolutionary aspect in having observed that these dsRNA viruses replicate associated to membranous organelles, a hallmark of +RNA viruses. However, we agree with the reviewer that this might not be the main point of our manuscript, so we reduced this paragraph accordingly. Please, see lines 358-367 in our revised version of the manuscript.

> *(16) Lines 322-324: Change "RdRd" to "RdRp" if keeping paragraph.*

Thanks. We have corrected this mistake in lines 360 and 361.

> *(17) Figures 1A, 1B, and throughout: Again, please check and explain protein sizes and amounts. This would improve the clarity of the manuscript.*

All our flotation assays were performed using 1 mM concentration of purified protein in a final volume of 100 mL (mentioned in M&M section). The complete fusion protein His-2xFYVE (shown in Figs. 1A and 4A left panel) is 954 base pairs-long and contains 317 residues (~35 kDa). The complete fusion protein His-VP3 FL (shown in Figs. 1B and 1G left panel) is 861 base pairs-long and contains 286 residues (~32 kDa). The complete fusion protein His-VP3 DCt (shown in Fig. 1G, right panel) is 753 bp-long and contains 250 residues (~28 kDa). The complete fusion protein His-VP3 FL $R_{200}D$ (shown in Fig. 4A right panel) is 861 bp-long and

contains 286 residues (~32 kDa). This latter information was incorporated in our revised version of the manuscript. Please, see lines 381-382, 396-397 and 399-400 from the M&M section, and lines in the corresponding figure legends.

> *(18) Figures 1B and 1G show different results for PI3P(+) membranes. I see protein associated with the top fraction in 1B, but I don't see any such result in 1G.*

As already mentioned, liposome-based methods, such as the co-flotation assay, are well-established and widely regarded as the preferred approach for studying protein-phosphoinositide interactions. However, this approach is rather qualitative, as density gradient separation reveals whether the protein is located in the top fractions (bound to liposomes) or the bottom fractions (unbound). Our quantifications aim to demonstrate differences in the bound fraction between liposome populations with and without PI3P. Given the setting of the co-flotation assays, each protein-liposome system [2xFYVE-PI3P(-), 2xFYVE-PI3P(+), VP3-PI3P(-), or VP3-PI3P(+)] is assessed separately, and even if the conditions are homogeneous, it's not surprising to observe differences in the protein level between each one. Indeed, the revised version of the manuscript include a membrane for Figure 1G, were His-VP3 FL associated with the top fraction is more clear. Please, see the new version of Figure 1G.

> *(19) Figure 1C: Please include cryo-EM images of the liposome PI3P(-) variables to assess the visual differences of the liposomal membranes under these conditions.*

Thanks for the recommendation. it has been verified that there is no binding of gold particles to liposomes PI3P(-) when they are incubated solely with the gold-particle reagent, or when they are pre-incubated with the gold-particle reagent with either His-2xFYVE or His-VP3 FL. We have incorporated a new panel in Figure 1C showing a representative image of these results. Please, see lines 143-144 in the revised version of our manuscript and our revised version of Figure 1C.

> *(20) Figures 2D, 2E, and 3A: The puncta are not obvious in these images. Consider adding Zoomed panels.*

We apologize for this aspect of Figures 2 and 3, also highlighted by reviewer #1. We believe that this was due to the low quality resulting from the PDF conversion of the original files. For Figure 3A, we have homogenized its aspect with those from 3B. Regarding Figure 2, we have incorporated zoomed panels, as suggested. Please, see the revised versions of both Figures.

> *(21) Figure 4A: There is almost no protein in the control PI3P(+) blot. Why? Also, the quantification shows no significant membrane association for this control. This result is different from Figure 1A and very confusing (and concerning).*

We apologize for the confusion. We replaced membranes for Figure 4A (left panel) with more similar band intensities to that shown in Figure 1A. Please, visit our new version of Figure 4. The quantification shows no significant difference in the association to liposomes PI3P(+) compared to liposomes PI3P(+); it's true and this is due to, once more, the intrinsically lack of homogeneity of co-flotation assays. However, this one shown in Figure 4A is a redundant control (has been shown in Figure 1A) and we believe that the new membrane is qualitative eloquent.

> ***Reviewer #3 (Recommendations For The Authors):***
>
> *(1) Overall, the title is general and does not summarize the study. I recommend making the title more specific. The current title is better suited for a review as opposed to a research article. This study provides further biophysical details on the interaction. This should be reflected in the title.*

We appreciate this recommendation, which was also expressed by reviewer #2. We have chosen a new title for the manuscript: “On the Role of VP3-PI3P Interaction in Birnavirus Endosomal Membrane Targeting”.

> *(2) References 8,9,10 are important but they were not correctly cited in the work, this should be corrected.*

We apologize for this mistake. These citations are identifiable in our revised version of the manuscript. See lines 100-105.

> *(3) Flotation experiments and cryo-EM convincingly show that VP3 binds to membranes in a PIP3-dependent manner. However, it would be advisable to include a control for cryo-EM using liposomes that do not contain PIP3 but are incubated with HIS-VP3-FL. This would allow us to rule out any unspecific binding that might not be detected on WB.*

Thanks for the advice, also given by reviewer #2. We confirmed that no gold particles were bound on liposomes PI3P(-) even when incubated with the Ni-NTA reagent alone or pre-incubated with His-2xFYVE of His-VP3 FL. We have incorporated a new panel to Figure 1C showing a representative image of these results. Please, see lines 143-144 in the revised version of the manuscript and see the revised version of Figure 1C.

> *(4) It is not clear what is the difference between WB in B and WB in G. Figure 1G seems to show the same experiment as shown in B, is this a repetition? In both cases, plots next to WBs show quantification with bars, do they represent STD or SEM? Legend A mentions significance p>0.01 (**) but the plot shows ***. This should be corrected.*

The Western blot membrane in Figure 1B shows the result of co-flotation assay using His-VP3 FL protein, while the Western blot membrane in Figure 1G (left panel) shows a co-flotation assay using His-VP3 FL protein as a positive control. In another words, in 1B the His-VP3 FL protein is the question while in 1G (left panel) it’s the co-flotation positive control for His-VP3 DCt. The bar plots next to Western blots show quantification, the mean and the STD. Thanks for highlighting this inconsistency. We have now corrected it on the revised version of the manuscript.

> *(5) It would be useful to indicate positively charged residues and P2 on the AF2 predicted structure in Fig 1.*

These are indicated in panels A and B of Figure 2.

> *(6) Figure 1 legend: Change cryo-fixated liposomes to cryo-fixation or better to "liposomes were vitrified". There is a missing "o" in the cry-fixation in the methods section.*

Thanks for the recommendation. We have modified Figure 1. legend to "liposomes were vitrified" (line 758), and fixed the word cryo-fixation in the methods section (line 512).

> *(7) Figure 2B. It is not clear how the punctated phenotype was unbiasedly characterized (Figure 2D). I see no difference in the representative images. Magnified images should be shown. This should be measured as colocalization (Pearson's and Mander's coefficient) with an early endosomal marker Rab5. Perhaps this figure could be consolidated with Figure 3.*

Unfortunately, the lack of clarity in Figure 2D was due to the PDF conversion of the original files. Please, observe the high-quality original image above in response to reviewer #1, where we have additionally included zoomed panels, as also suggested by the other reviewers. For quantification of the co-localization of VP3 and either EGFP-Rab5 orEGFP-2xFYVE, the Manders M2 coefficient was calculated out of approximately 30 cells per construct and experiment and were shown in Figure S3 and Figure 3A, respectively, in our previous version of the manuscript.

> *(8) PIP3 antagonist drugs should be used to further substantiate the results. If PIP3 specifically recruits VP3, this interaction should be abolished in the presence of PIP3 drug and VP3 should show a diffused signal.*

We certainly agree with this point. These experiments were performed and the results were reported in (Gimenez et al., 2020). Briefly, in that work, we blocked the synthesis of PI3P in QM7 cells in a stable cell line overexpressing VP3, QM7-VP3, with either the pan-PI3Kinase (PI3K) inhibitor LY294002, or the specific class III PI3K Vps34 inhibitor Vps34-IN1. In Figure 4, we showed that 98% of the cells treated with these inhibitors had the biosensor GFP-2FYVE dissociated from EEs, evidencing the depletion of PI3P in EEs (Figure 4A). In QM7-VP3 cells, we showed that the depletion of PI3P by either inhibitor caused the dissociation of VP3 from EEs and the disaggregation of VP3 puncta toward a cytosolic distribution (Figure 4B). Moreover, since this observation was crucial for our hipothesis, these results were further confirmed with an alternative strategy to deplete PI3P in EEs. We employed a system to inducibly hydrolyze endosomal PI3P through rapamycin-induced recruitment of the PI3P-myotubularin 1 (MTM1) to endosomes in cells expressing MTM1 fused to the FK506 binding protein (FKBP) and the rapamycin-binding domain fused to Rab5, using the fluorescent proteins mCherry-FKBP-MTM1 and iRFP-FRB-Rab5, as described in (Hammond et al., 2014). These results, shown in Figures 5, 6 and 7 in the same manuscript, further reinforced the notion that PI3P mediates and is necessary for the association of VP3 protein with EEs.

> *(9) The authors should show the localization of VP3 in IBDV-infected cells and treat cells with PI3P antagonists. The fact that R_{200} is not rescued does not necessarily mean that this is because of the failed interaction with PI3P. As the authors wrote in the discussion: VP3 bears multiple essential roles during the viral life cycle (line 305).*

Indeed, after having confirmed that the VP3 lost its localization associated to the endosomes after the treatment of the cells with PI3P antagonists, we demonstrated that depletion of PI3P significantly reduced the production of IBDV progeny. For this aim, we used two approaches, the inhibitor Vps34-IN1 and an siRNA against VPs34. In both cases, we observed a significantly reduced production of IBDV progeny (Figures 9 and 10). Specifically related to the reviewer's question, the localization of VP3 in IBDV-infected cells and treated with PI3P antagonists was shown and quantified in Figure 9a.

> *(10) Could you provide adsorption-free energy profiles and MD simulations also for the R_{200} mutant?*

Following the reviewer's suggestion, we have added a new figure to the supplementary information (Figure S15). Instead of presenting a full free-energy profile for each protein, we

focused on the adsorption free energy (i.e., the minimum of the adsorption free-energy profile) for VP3 ΔNt and its mutants, VP3 ΔNt $R_{200}D$ and VP3 ΔNt P2 Mut, as a function of salt concentration. The aim was to compare the adsorption free energy of the three proteins and evaluate the effect of electrostatic forces on it, which become increasingly screened at higher salt concentrations. As shown in the referenced figure, reducing the number of positively charged residues from VP3 ΔNt to VP3 ΔNt P2 Mut systematically weakens the protein's binding to the membrane. This effect is particularly pronounced at lower salt concentrations, underscoring the importance of electrostatic interactions in the adsorption of the negatively charged VP3 onto the anionic membrane.

> *(11) Liposome deformations in the presence of VP3 are interesting (Figure 6G), were these also observed in Figure 1C?*

Good question. The liposome deformations in the presence of VP3 shown in Figure 6G were a robust observation since, as mentioned, it was detectable in 36% of the liposomes PI3P(+), while they were completely absent in PI3P(-) liposomes. However, and unfortunately, the same deformations were not detectable in experiments performed using gold particles shown in Figure 1C. In this regard, we think that it might be possible that the procedure of gold particles incubation itself, or even the presence of the gold particles in the images, would somehow "mask" the deformations effect.

Bibliography

Boukhalfa A, Roccio F, Dupont N, Codogno P, Morel E. 2021. The autophagy protein ATG16L1 cooperates with IFT20 and INPP5E to regulate the turnover of phosphoinositides at the primary cilium. *Cell Rep* 35:109045. doi:10.1016/j.celrep.2021.109045

Casañas A, Navarro A, Ferrer-Orta C, González D, Rodríguez JF, Verdaguer N. 2008. Structural Insights into the Multifunctional Protein VP3 of Birnaviruses. *Structure* 16:29–37. doi:10.1016/j.str.2007.10.023

Delgui LR, Rodriguez JF, Colombo MI. 2013. The Endosomal Pathway and the Golgi Complex Are Involved in the Infectious Bursal Disease Virus Life Cycle. *J Virol* 87:8993–9007. doi:10.1128/JVI.03152-12

Gimenez MC, Issa M, Sheth J, Colombo MI, Terebiznik MR, Delgui LR. 2020. Phosphatidylinositol 3-Phosphate Mediates the Establishment of Infectious Bursal Disease Virus Replication Complexes in Association with Early Endosomes. *J Virol* 95:e02313-20. doi:10.1128/jvi.02313-20

Hammond GRV, Machner MP, Balla T. 2014. A novel probe for phosphatidylinositol 4-phosphate reveals multiple pools beyond the Golgi. *J Cell Biol* 205:113–126. doi:10.1083/jcb.201312072

Khaldoun SA, Emond-Boisjoly MA, Chateau D, Carrière V, Lacasa M, Rousset M, Demignot S, Morel E. 2014. Autophagosomes contribute to intracellular lipid distribution in enterocytes. *Mol Biol Cell* 25:118. doi:10.1091/mbc.E13-06-0324

Luque D, Saugar I, Rejas MT, Carrascosa JL, Rodríguez JF, Castón JR. 2009. Infectious Bursal Disease Virus: Ribonucleoprotein Complexes of a Double-Stranded RNA Virus. *J Mol Biol* 386:891–901. doi:10.1016/j.jmb.2008.11.029

Morel E, Chamoun Z, Lasiecka ZM, Chan RB, Williamson RL, Vetanovetz C, Dall'Armi C, Simoes S, Point Du Jour KS, McCabe BD, Small SA, Di Paolo G. 2013. Phosphatidylinositol-3-phosphate regulates sorting and processing of amyloid precursor protein through the endosomal system. *Nature Communications 2013 4:1* 4:1–13. doi:10.1038/ncomms3250

Qi X, Gao Y, Gao H, Deng X, Bu Z, Wang Xiaoyan, Fu C, Wang Xiaomei. 2007. An improved method for infectious bursal disease virus rescue using RNA polymerase II system. *J Virol Methods* 142:81–88. doi:10.1016/j.jviromet.2007.01.021

https://doi.org/10.7554/eLife.97261.2.sa0